REVIEW ARTICLE | APRIL 24 2025

Polarization and domains in wurtzite ferroelectrics: Fundamentals and applications

Simon Fichtner ; Georg Schönweger ; Cheng-Wei Lee ; Keisuke Yazawa ; Prashun Gorai ; Geoff L. Brennecka

Appl. Phys. Rev. 12, 021310 (2025)
https://doi.org/10.1063/5.0249265
CHORUS

Applied Physics Reviews REVIEW pubs.aip.org/aip/are

Polarization and domains in wurtzite ferroelectrics: Fundamentals and applications

Cite as: Appl. Phys. Rev. **12**, 021310 (2025); doi: 10.1063/5.0249265
Submitted: 16 November 2024 · Accepted: 8 April 2025 ·
Published Online: 24 April 2025

Simon Fichtner,[1,2,a)] Georg Schönweger,[1,2] Cheng-Wei Lee,[3] Keisuke Yazawa,[3,4] Prashun Gorai,[3,4,5] and Geoff L. Brennecka[3,a)]

AFFILIATIONS

[1]Kiel University, Kiel, Germany
[2]Fraunhofer Institute for Silicon Technology, Itzehoe, Germany
[3]Colorado School of Mines, Golden, Colorado 80401, USA
[4]National Renewable Energy Laboratory, Golden, Colorado 80401, USA
[5]Rensselaer Polytechnic Institute, Troy, New York 12180, USA

[a)]**Authors to whom correspondence should be addressed:** sif@tf.uni-kiel.de and geoff.brennecka@mines.edu

ABSTRACT

The 2019 report of ferroelectricity in (Al,Sc)N [Fichtner *et al.*, J. Appl. Phys. **125**, 114103 (2019)] broke a long-standing tradition of considering AlN the textbook example of a polar but non-ferroelectric material. Combined with the recent emergence of ferroelectricity in HfO_2-based fluorites [Böscke *et al.*, Appl. Phys. Lett. **99**, 102903 (2011)], these unexpected discoveries have reinvigorated studies of integrated ferroelectrics, with teams racing to understand the fundamentals and/or deploy these new materials—or, more correctly, attractive new capabilities of old materials—in commercial devices. The five years since the seminal report of ferroelectric (Al,Sc)N [Fichtner *et al.*, J. Appl. Phys. **125**, 114103 (2019)] have been particularly exciting, and several aspects of recent advances have already been covered in recent review articles [Jena *et al.*, Jpn. J. Appl. Phys. **58**, SC0801 (2019); Wang *et al.*, Appl. Phys. Lett. **124**, 150501 (2024); Kim *et al.*, Nat. Nanotechnol. **18**, 422–441 (2023); and F. Yang, Adv. Electron. Mater. **11**, 2400279 (2024)]. We focus here on how the ferroelectric wurtzites have made the field rethink domain walls and the polarization reversal process—including the very character of spontaneous polarization itself—beyond the classic understanding that was based primarily around perovskite oxides and extended to other chemistries with various caveats. The tetrahedral and highly covalent bonding of AlN along with the correspondingly large bandgap lead to fundamental differences in doping/alloying, defect compensation, and charge distribution when compared to the classic ferroelectric systems; combined with the unipolar symmetry of the wurtzite structure, the result is a class of ferroelectrics that are both familiar and puzzling, with characteristics that seem to be perfectly enabling and simultaneously nonstarters for modern integrated devices. The goal of this review is to (relatively) quickly bring the reader up to speed on the current—at least as of early 2025—understanding of domains and defects in wurtzite ferroelectrics, covering the most relevant work on the fundamental science of these materials as well as some of the most exciting work in early demonstrations of device structures.

TABLE OF CONTENTS

I. INTRODUCTION

Ferroelectrics allow nonvolatile charge control by switching the spontaneous polarization on a unit cell level through external electric fields. This ability makes them one of the most self-evident approaches for information storage in nanoelectronics. Unlike other purely charge based nonvolatile solutions, ferroelectric memory is not inherently reliant on *defects* such as trapped charges or mobile ions, thereby offering potentially much improved endurance as well as reduced energy demand. Equally important, ferroelectrics are truly multi-functional, being necessarily pyroelectric and piezoelectric, as well as optically non-linear. As ferroelectricity is the result of a polar (i.e., low symmetry) unit cell, different crystal structures can behave vastly differently in terms of their suitability for a particular application. The realization of ferroelectricity in a crystal class previously considered non-ferroelectric can therefore greatly enhance our technological possibilities. Consequently, the 2019 discovery that thin films with wurtzite structure can exhibit ferroelectric properties has further invigorated research into ferroelectrics and their applications in micro- and nanoelectronics. Together with the 2009 discovery of ferroelectric fluorite-structured HfO_2 films and steadily growing sophistication with respect to perovskite ferroelectrics, the field today is more diverse than it has ever been.[1–9]

The wurtzite structure served for a long time as a textbook example of a polar, yet not ferroelectric, structure. Aside from the application potential of wurtzite ferroelectrics, therefore, researchers are intrigued by how ferroelectric switching occurs in this material class previously assumed to be unswitchable—in particular, how does the polarization inversion manifest on the atomic scale? In this paper, we review the current understanding of how polarization switching is enabled on unit- and supercell level in wurtzite-structured compounds and alloys and how ferroelectric polarization switching progresses in real thin films. In addition, we provide a brief overview of the emerging applications that benefit from ferroelectricity in wurtzite thin films.

Section II starts with a general introduction to spontaneous polarization $\mathbf{P_s}$ and how the lack of a uniquely defined expression from first principles has complicated our understanding of $\mathbf{P_s}$ in the wurtzite structure in the past. This is followed by a discussion of the experimental evidence for domain formation during ferroelectric switching of wurtzite materials. Subsequently, we review how the mechanisms of ferroelectric polarization inversion are described based on density functional theory (DFT) calculations, how these mechanisms differ for different chemistries, as well as what determines the possibility of a certain wurtzite material being ferroelectric and thus of interest for future experimental studies. Section III discusses experimentally derived ferroelectric properties and how these compare to more established classes of ferroelectric thin film materials. Aside from the basic polarization vs electric field dependency, this includes a discussion of wake-up and imprint. Section IV then summarizes current approaches to harness the ferroelectric properties of wurtzite materials for new and improved applications in the context of memory, resonators, optoelectronics, and actuators.

II. SPONTANEOUS POLARIZATION AND DOMAINS

A. Spontaneous polarization in crystals

The polarization $\mathbf{P}$ of a dielectric material describes the charge separation that occurs due to the presence of an external electric field $\mathbf{E}$. Together, they result in the dielectric displacement field $\mathbf{D}$, according to

$$\mathbf{D} = \epsilon_0\mathbf{E} + \mathbf{P}(E) \underset{\text{for linear dielectrics}}{=} \epsilon_0\epsilon_r\mathbf{E}, \quad (1)$$

where ϵ_0 and ϵ_r are the vacuum and relative permittivity, respectively. In addition to electric field-induced polarization, materials whose crystallographic symmetry can be described by 1 of 10 polar point groups exhibit a spontaneous polarization $\mathbf{P_s}$. As such, materials with spontaneous polarization (pyroelectrics, because the magnitude of $\mathbf{P_s}$ varies with temperature) are non-centrosymmetric, piezoelectric, and symmetrically indistinguishable from ferroelectrics—the latter being pyroelectrics whose $\mathbf{P_s}$ can be switched by external electric fields. *Thus, ferroelectrics are simply an experimentally-determined subset of pyroelectrics.*

For a finite charge distribution $\rho(\mathbf{r})$ as in a standalone molecule, $\mathbf{P_s}$ (or rather, the dipole moment) is given by its integral over the considered volume weighted by the position $\mathbf{r}$

$$\mathbf{P} = \int_V \rho(\mathbf{r})\mathbf{r}d\mathbf{r}. \quad (2)$$

In bulk crystals, the treatment of $\mathbf{P}$ is more complex. Nonetheless, the quantity remains an intrinsic property of the material and can be calculated using the modern theory of polarization (MTP).[10,11] The complexity in bulk crystals arises from the fact that the magnitude and direction of $\mathbf{P_s}$ cannot be uniquely defined. From an experimental point of view, this is a moderate concern since only differences in $\mathbf{P_s}$ can be measured, and these differences are well-defined in the MTP framework.

To illustrate why there is no unique definition for the value and direction of $\mathbf{P_s}$, while there is one for $\Delta\mathbf{P_s}$, we follow the intuitive graphical explanation given by Spaldin:[12] Fig. 1 gives a simple example of a spontaneously polarized *crystal* in the form of a non-centrosymmetric chain of charges. Clearly, the magnitude and direction of the $\mathbf{P_s}$ depend on the choice of the unit cell. This ambiguous $\mathbf{P_s}$ changes when we consider, e.g., the displacement of one of the charges relative to the other, i.e., induce a change in the lattice, while keeping the previous unit cell definitions (Fig. 2). This situation is comparable to the direct piezoelectric effect (strain induced displacement) or to an electric field induced polarization change. While sign and magnitude of $\mathbf{P_s}$ still differ for both unit cell definitions after the displacement, the resulting change $\Delta\mathbf{P_s}$ is equal in both cases. Thus, $\Delta\mathbf{P_s}$ is unambiguous in magnitude and sign. For theoretical calculations in the framework of the MTP, this implies that these calculations must always be performed relative to some reference structure. The choice of this reference structure is thus crucial for defining the absolute $\mathbf{P_s}$. This is not merely an academic question, as such polarization is key to high electron mobility transistors (HEMTs) and other devices discussed in Sec. IV. This initial choice of reference structure has caused significant misunderstanding in the case of the wurtzite crystal structure, as corrected by Dreyer *et al.*[13]

Experimentally, the most common way to measure spontaneous polarization is ferroelectric switching. Consequently, the polarization

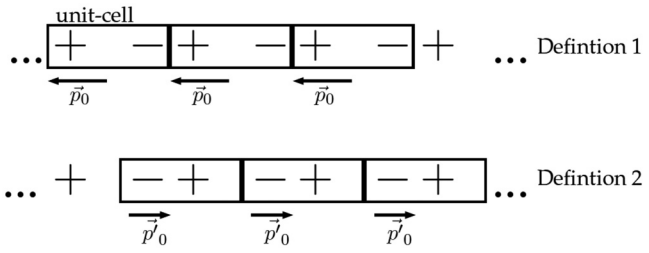

FIG. 1. Sketch of non-centrosymmetric one-dimensional *crystal* and two possible choices for a unit cell to illustrate the ambiguous nature of $\mathbf{P_s}$: The direction and magnitude of $\mathbf{P}$ directly depends on this unit cell choice.

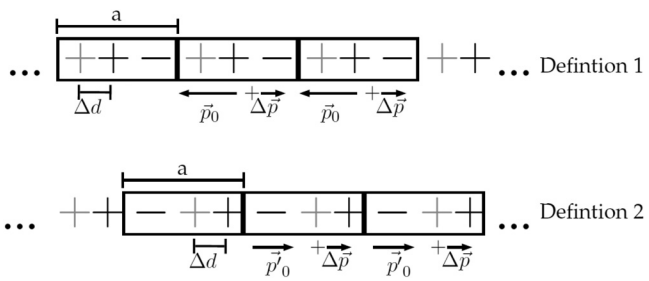

FIG. 2. Sketch of the same crystal as in Fig. 1 using the same unit cell definitions, after undergoing a constant displacement of the positive charges with respect to the negative charges by Δd, e.g., due to strain or an electric field. While the magnitude and the direction of $\mathbf{P_s}$ still differ, the resulting polarization change $\Delta\mathbf{P}$ is equal and thus well-defined for both definitions. Note that we here use the convention of polarization being defined as negative-to-positive, though this convention occasionally varies with technical community.

magnitude of wurtzite-type compounds was only determined accurately once their ferroelectric characteristics became known.[1] When determining $\mathbf{P_s}$ from a polarization-vs-electric field loop, the reference structure is usually the structure with opposite polarity, i.e., the unit cell mirrored normal to the spontaneous polarization. According to Eq. (1), a change in polarization is accompanied by a change in dielectric displacement, which in turn gives rise to a measurable current density $\mathbf{j} = \frac{d}{dt}\mathbf{D}$. This current density can be integrated according to Eq. (3) to receive the switching polarization $\mathbf{P}_{sw}$, which one typically assumes to be twice the remanent polarization $\mathbf{P_r}$, which in turn can be a good approximation of $\mathbf{P_s}$. For a wurtzite-structured nitride having only two polarization states (metal, *M*- and nitrogen, *N*-polar; P_M and P_N; see Figs. 4 and 7 for illustrations), the integral for the determination of the switching polarization from the current density $\mathbf{j}$ would take the following form:

$$2\mathbf{P_s} = \mathbf{P_{SW}} = \mathbf{P_M} - \mathbf{P_N} = \int_{t\,\text{at}\,P_N}^{t\,\text{at}\,P_M} \left(\mathbf{j}(t) - \epsilon_0 \frac{d}{dt}\mathbf{E}\right) dt, \qquad (3)$$

when switching from *N*- to *M*-polarity. In case $\mathbf{E}(t)$ is the same for both integration limits, it can be neglected from the equation. The fact that two integration constants are required to solve a definite integral directly implies that polarization at any stage of ferroelectric switching can only be measured relative to a reference. By substitution, $\mathbf{P_{sw}}(\mathbf{E})$ can be determined, which is commonly plotted symmetric around the electric field axis, so that both negative and positive $\mathbf{P_r}$ have the same magnitude.

Since in parallel plate capacitor structures, both $\mathbf{P_{sw}}$ and $\mathbf{E}$ are evaluated along their 3- or out-of-plane direction, vector (component) notation is uncommon for plotting polarization vs electric field (PE) loops.

B. Spontaneous polarization in the wurtzite structure

The spontaneous polarization lies along the *c*-axis of the wurtzite structure, which is referred to as the polar axis. Wurtzite-type thin films typically grow with preferred *c*-axis orientation, i.e., the polar axis is aligned perpendicular to the film surface. For an electric field applied directly normal to the film surface (again assuming a parallel plate configuration), deviation of the polar axis from the out-of-plane direction reduces the field applied along the polar direction to the cosine of the total field. The magnitude of P_s depends on both the atomic species involved and the internal distortion of the wurtzite structure, which is typically quantified by the internal parameter u. This value amounts to the distance between the nitrogen and the metal atom along the *c*-direction relative to the unit cell and correlates therefore to the magnitude of the dipole moment. Any increase in u (due to, e.g., alloying or strain) reduces P_s until the wurtzite structure transforms at $u = 0.5$ theoretically into the non-polar ($P_s = 0$) layered hexagonal structure. This intermediate state is—at least conceptually, if not literally—considered to be the transition state when switching from one polarity to the other. Thus, it is intuitive that an increase in u correlates with a decrease in the energy barrier for polarization inversion. The as-grown polarity (i.e., M- or N-polarity) of wurtzite-type materials such as GaN, InN, and AlN can be tuned through growth conditions and/or the substrate or layer onto which the initial film is grown. Because of the direct link between polarity and functionality for many potential III-N devices (e.g., the polarization discontinuity in HEMTs), growth polarity is especially important for non-ferroelectric materials, as any disturbance of the unipolar polarization state will degrade electrical and/or optical performance. However, regions with opposing polarity (inversion domains) are a common phenomenon in as-grown wurtzite-type materials such as GaN.

C. Ferroelectric polarization domains

Polarization domains in ferroelectrics can be defined as regions with different directions of spontaneous polarization, yet otherwise comparable structural and chemical properties. They can be formed during material synthesis, through external electric fields during ferroelectric switching, during phase transitions and/or through time- or temperature-induced depolarization. Key questions about the nature, structure, and dynamics of domains and domain walls remain open, as do questions about the multiple potential effects of point and extended defects and interfaces across all ferroelectrics, and additionally so in the emerging fluorite and wurtzite ferroelectrics.

Even though nomenclature suggests otherwise, polarization domains in ferroelectrics and their dynamics differ greatly from domains in ferromagnets, as has been observed since the early days of ferroelectrics:[14] while domain walls in ferromagnets can have thicknesses in the range of tens of nm, domain walls in ferroelectrics are often found to be very thin, even down to atomically sharp.[15–17] Consequently, domains themselves in ferroelectrics can be substantially smaller than domains in ferromagnets (down to a few nm^3), which implies that domain nucleation may occur much more frequently in ferroelectrics.[14,18]

The fact that spontaneous polarization can be readily screened by often abundant monopoles (e.g., electrons, holes, or charged ionic species) has the consequence that closure domains are often not required to limit stray fields again, unlike in ferromagnets, where the absence of monopoles leads to more complex surface domain patterns.[15] The compensation of polarization charge by screening charges has important implications for the types of domain walls that can be observed in ferroelectrics as well as the dynamic evolution of such domain structures.

Intuitively, domain walls that are directly compensated by the polarization of neighboring domains or are aligned parallel to the polar axis should be most stable, as this does not require an additional electrostatic energy contribution. However, charged domain walls are a common occurrence[15,19] (see Fig. 3). These charged domain walls can be screened locally through, e.g., electrons (head-to-head domain walls, positive polarization charge), holes (tail-to-tail domain walls, negative polarization charge), or potentially by charged ionic species. Screening is sufficient to stabilize huge polarization sheet charges, which can, for example, reach $> 100\mu$ C/cm^2 (or more than 15 electrons per nm^2) in $BiFeO_3$[20] as well as in wurtzite ferroelectrics, as discussed below. Usually, compensation charges in ferroelectric domain walls are mobile themselves, which essentially makes a charged domain wall conductive, and thus of great interest for resistive switching applications.[15,19,20]

When discussing domains in wurtzites, it is tempting to start from the more mature understanding of ferroelectricity in octahedrally coordinated perovskites and related structures, but one must not force an equivalence. For example, samples of the prototype ferroelectric $BaTiO_3$ are (almost) always fabricated (deposited, sintered, etc.) at temperatures above the $BaTiO_3$ Curie temperature (T_C) of $\sim 125\,^\circ$C, thus the material at room temperature cooled at some point in its history from a nonpolar phase into the polar phase of interest, developing in the process a non-trivial domain structure to reduce excess energy as best feasible given the particular electrical and mechanical boundary conditions of the particular sample and its processing history.

Wurtzites, however, are fabricated in their polar phase due to the extreme temperature stability of this phase.[21] As a consequence, electrical compensation associated with any discontinuities due to the spontaneous polarization can be present *during fabrication* rather than appearing during post-fabrication cooling at a temperature where long-range atomic mobility is quite limited. In addition, crystallographic symmetry of the 6mm point group to which AlN and other wurtzites belong limits the spontaneous polarization to the $\pm$c axis, eliminating the possibility for ferroelastic (and potentially flux-closing) non-180° domain walls. An important question arises, though: if polar wurtzites never go through a Curie temperature (i.e., undergo a nonpolar → polar phase transition), are polar domains necessary in such films?

A thought experiment can be illustrative. We imagine an ideal, defect-free wurtzite lattice in which the polarization is oriented up relative to the page. For simplicity, we focus on cation-centered tetrahedra. If the entire structure collectively and simultaneously became less polar (i.e., the cations moved closer to the basal plane), attained a nonpolar hexagonal boron nitride (hBN)-type phase, then proceeded to increase polarization in the opposite polarity (i.e., the cations emerged below the basal plane and gradually returned to their equilibrium location within the now downward-pointing tetrahedra, as represented in the left subfigure of Fig. 4), such a process would not necessarily require the nucleation and growth of new domains or the formation of discrete domain walls. In fact, studies have looked at the energetics of exactly this process.[22]

Alternatively, the nucleation and growth of oppositely-oriented domains requires—even if briefly—the formation of domain walls, of which there are a minimum of two types. One we will refer to as vertical domain walls because in our thought experiment they are oriented vertically through the crystal, forming a lateral separation of up - down polarities, originally described by Blank *et al.*[23] as shown in the right of Fig. 4. The other minimal domain wall would extend laterally through the crystal and would be described as either head-to-head or tail-to-tail in ferroelectrics parlance depending upon whether the polarizations both point toward or away from the wall. Of course, neither of these is a purely hypothetical interface; they are the inversion domain boundaries (IDBs) that GaN (and other) growers try to avoid (Fig. 5).[24,25] Thus, the earlier question of whether or not domains are required is essentially moot; whether required or not, they exist in real samples, so a better understanding is warranted.

The purportedly high energetic cost of head-to-head or tail-to-tail domain walls typically drives long needle or sharp ellipsoid-like structures that grow rapidly along the polarization direction[14] and much more slowly in lateral directions, which results in cylindrical domain shapes.[26,27] Occasionally, domain patterns have been reported whose formation did not follow these simple models, for example, forming broad cone-like domain shapes[28,29] and indicating a deviation from the simple compensation models represented in Figs. 3 and 5.

We now know that the polarization of wurtzites can be inverted through the application of an electric field, and we know how static, as-grown boundaries between oppositely charged domains can be structured. However, the structure and character of field-induced polarization domain walls in wurtzites remains under investigation. Recently, such electrically-induced domain walls have been directly

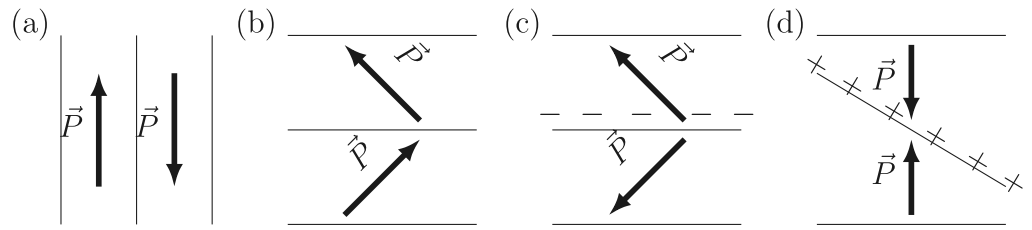

FIG. 3. Sketches to illustrate the concept of charged and uncharged domain walls in ferroelectrics: (a) uncharged 180° wall, (b) uncharged 90° wall, (c) charged tail-to-tail (negative sheet charge) 90° domain wall, and (d) charged head-to-head (positive sheet charge) 180° domain wall.

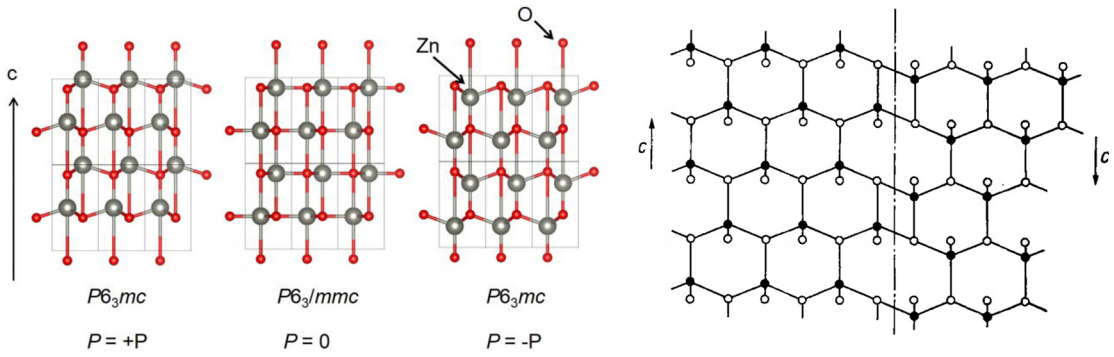

FIG. 4. Schematic illustration of (left) polarity inversion in a wurtzite via an intermediate nonpolar hexagonal structure. Reproduced with permission from Moriwake *et al.*, Appl. Phys. Lett. **104**, 242909 (2014).[22] Copyright 2014 AIP Publishing LLC. Schematic illustration of (right) a stacking fault between regions of opposite polarity in an otherwise-coherent wurtzite crystal, in other words, a domain wall. Reproduced with permission from Blank *et al.*, Phys. Status Solidi (b) **7**, 747 (1964).[23] Copyright 2006 John Wiley and Sons.

imaged, first in (Al,B)N (Fig. 6)[30] and soon after in (Al,Sc)N (Fig. 7).[31,32] While these TEM studies were conducted very differently (*ex situ* with voltage applied through a capacitor vs *in situ* with electric voltage applied through beam induced charging), they clearly demonstrate the existence and stability of domain walls induced through ferroelectric switching in the wurtzite structure. In each study, this stability is in spite of the presence of domain walls with a horizontal component, and thus (due to the unipolar nature of the wurtzite structure), strong polarization discontinuities. Furthermore, particularly for (Al,B)N, it was suggested that a nonpolar supercell is forming during the process of polarization inversion, implying that the unit cells do not pass through the presumed hBN intermediate structure after all.

The TEM specimens have significantly different boundary conditions than the as-fabricated films, and both through-foil projection artifacts and sampling statistics demand caution when extrapolating quantitatively from such images. However, it is striking that both Calderon *et al.*[30] and Schönweger *et al.*[31] show domain walls that are more complex than originally suggested by Fichtner *et al.*[1] based upon the earlier work from Moriwake *et al.*[22] In fact, recent computational work has also suggested that the simple hBN-like switching mechanism may be the lowest-energy inversion pathway for only a minority of wurtzite ferroelectrics.

D. Switching pathways

The hBN-like structure is now broadly accepted as an appropriate nonpolar prototype for wurtzite ferroelectrics from a polarization calculation perspective, including not only the original $Al_{1-x}Sc_xN$,[1] but also $Al_{1-x}B_xN$,[33] $Al_{1-x}Y_xN$,[34] $Zn_{1-x}Mg_xO$,[35] $Ga_{1-x}Sc_xN$,[36,37] and $Al_{1-x}Gd_xN$,[38] with more chemistries sure to be added to the list in coming months and years. It is important to remember, however, that there is no requirement that the polarization reversal process in real materials actually pass collectively through the prototype nonpolar phase as an intermediate stage.

In parallel with recent direct experimental evidence of domain walls in wurtzite-type AlN-based alloys, computational studies provide insights into the inversion pathways at an atomic scale. While early computational works[13,22] relied on symmetry analysis to deduce the nonpolar intermediate structure along a hypothetical switching pathway between positive (wz^+) and negative polarities (wz^-) of the wurtzite structure, recent computational studies have utilized the nudged elastic band (NEB) method, to find the minimum energy path (MEP) between wz^+ and wz^-.[30,39–47] For binary wurtzite compounds including AlN and ZnO, all reported NEB-based predictions find the same switching pathway as the one based on symmetry analysis: $wz^+ \rightarrow hex^0 \rightarrow wz^-$, where hex^0 is the nonpolar ($P = 0$) layered hexagonal structure shown in Figs. 4 and 8.

However, there is growing evidence that this switching pathway is not the MEP for materials of increased chemical diversity. Lee *et al.* performed a systematic study on the inversion pathway of $Al_{1-x}Sc_xN$ ($0 < x < 0.44$) using solid state NEB (SS-NEB, which allows both cell shape and size to vary and therefore represents a more generalized version of NEB[43]) methods and found that the switching mechanism depends on the Sc composition as shown in Figs. 8(a) and 8(b).[39] At low Sc compositions ($x \lesssim 0.28$), the inversion process follows the "collective" or "uniform coherent" switching of the wz^+–hex^0–wz^- pathway, while at high Sc compositions ($x \gtrsim 0.28$) polarization inversion occurs via "individual" or "sequential" switching of discrete tetrahedra. The new pathways are named after their distinct behaviors at the atomic scale: individual cation-centered tetrahedra switch their polarities sequentially as shown in Fig. 8(c).

Lee *et al.* also studied $Al_{1-x}B_xN$ and $Al_{1-x}Gd_xN$ to further understand the composition–structure–property relationship of ferroelectric AlN-based alloys. They found that the predicted critical alloying compositions at which the switching mechanism changes from "collective" for the AlN-rich alloys to "individual" for the alloys with greater Al substitution are comparable to the alloying composition at which polarization inversion was experimentally observed at or near room temperature in subsequent experimental work.[38] It is important to note that because polarization reversal depends upon the ratio of coercive field to breakdown field, both of which vary with extrinsic factors, there is no such thing as a critical composition for which ferroelectricity is or is not possible, but such computational guidance can highlight when intrinsic barriers suggest easier or more difficult experimental realization of ferroelectricity. Similar conclusions were also

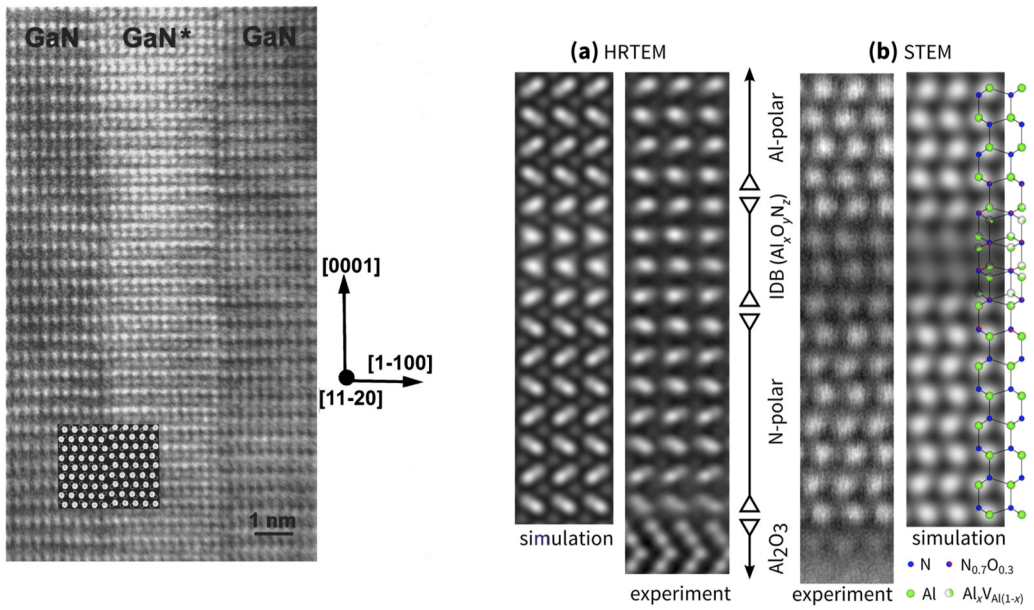

FIG. 5. TEM image of (left) vertical and (right) oxygen induced horizontal inversion domain boundaries in wurtzite GaN. Both inversion domain boundaries were introduced during growth. Left: Reproduced with permission from Romano *et al.*, Appl. Phys. Lett. **69**, 2394–2396 (1996).[24] Copyright 1996 AIP Publishing LLC. Right: Reproduced with permission from Mohn *et al.*, Phys. Rev. Appl. **5**, 054004 (2016).[25] Copyright 2016 Authors, licensed under a Creative Commons Attribution (CC BY 3.0) license.

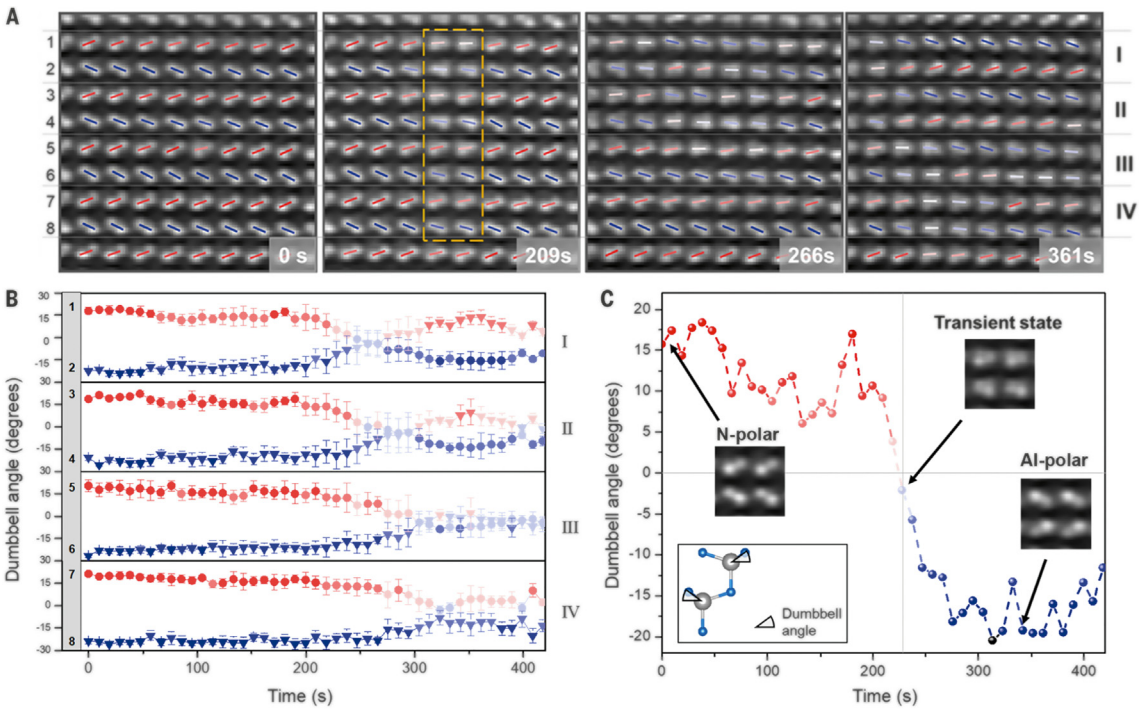

FIG. 6. TEM images and associated displacement tracking of beam-induced polarity inversion in $Al_{0.94}B_{0.06}N$. Reproduced with permission from Calderon *et al.*, Science **380**, 1034–1038 (2023).[30] Copyright 2023 The American Association for the Advancement of Science.

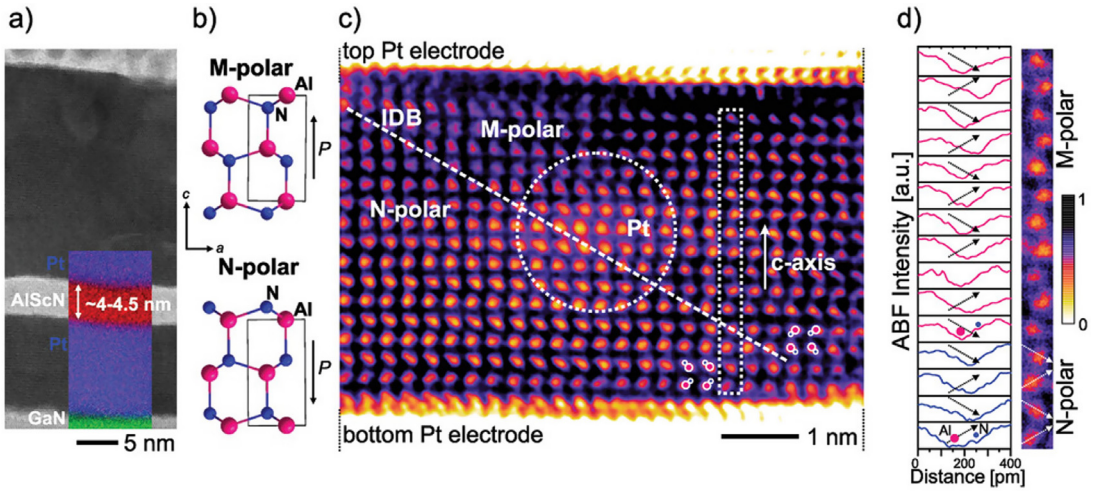

FIG. 7. TEM images and associated displacement tracking in a partially switched region of an $Al_{0.74}Sc_{0.26}N$ film showing a laterally extended domain wall. Reproduced with permission from Schönweger *et al.*, Adv. Sci. **10**, 2302296 (2023).[31] Copyright 2023 Authors, licensed under a Creative Commons Attribution (CC BY 4.0) license.

independently derived based on computational results of $Zn_{1-x}Mg_xO$ by Baksa *et al.*[47] Higher Mg substitution amounts introduce stronger local structural distortion to ZnO and thus larger strain fluctuations, which promote change in switching mechanism and a reduction in coercive field. Based on this, they proposed that strain fluctuations and coercive fields can be controlled via synthesis of ZnO/MgO heterostructures or introducing Mg composition gradients along the polar direction.

One key difference of individual switching from the collective pathway is the intermediate nonpolar structures. Collective switching generally proceeds through a transient nonpolar structure, which is either at the saddle point or the shallow local minimum of the MEP (see AlN and $Al_{0.78}Sc_{0.22}N$ alloy in Fig. 8). In contrast, individual switching profiles have multiple (relatively) deep local minima along the MEPs. A nonpolar structure consisting only of tetrahedra has exactly half of each polarity. Such new nonpolar structures were predicted and experimentally identified recently by multiple groups. Liu *et al.* performed standard NEB calculations on a 32-atom supercell based on the special quasi-random structure approach and found that $Al_{1-x}B_xN$ alloys with $x > 0.0625$ exhibit a β-BeO-like nonpolar structure, shown in Fig. 8(d).[41] Similarly, Calderon *et al.* imaged the same nonpolar structure and associated it with the inversion domain boundary commonly observed in nitrides.[30] They further supported the observed boundary with NEB calculations as shown in Fig. 8(e). Most recently, Lee *et al.* identified five unique nonpolar structures, as shown in Fig. 8(f), among the candidate wurtzite-derived multinary compounds they found in their earlier computational search.[39,40] Two of these can be associated with known crystal structures—β-BeO and cubanite (Fe_2CuS_3-type) structures—while the rest are newly reported. These structures can presumably be mapped onto the local structures of (horizontal) domain walls, though this point awaits additional experimental confirmation.

Finally, while NEB calculations based on first-principles methods like DFT provide useful insights into inversion pathways and the identified nonpolar structures could be mapped onto static domain walls, a critical gap still exists between experimental observables like coercive field and first-principles predictions. Specifically, it remains computationally intractable to simulate domain wall motion using first-principles methods like DFT since it requires thousands of unit cells with explicit external electric field. However, emerging developments in machine-learned interatomic potentials are expected to be useful for enabling multiscale simulations that bridge this scale gap in the near future.[48,49]

E. Chemistries

The enormous coercive fields (more specifically, the proximity of typical coercive fields to typical breakdown fields) is the primary reason that the wurtzite ferroelectrics were discovered so much later than their octahedrally coordinated cousins. While large switching barriers can be advantageous for stability and retention, small margins between switching and breakdown are potentially problematic for devices, and integration with low-power devices demands low voltage operation. Thus, finding ways of reducing the switching energy barriers in such materials has led researchers to explore new chemistries.

Traditionally, exploration of new chemistries has been driven by chemical intuition and empirical observations. Within the wurtzite ferroelectrics, the typical approach has been to alloy binary wurtzites like AlN and ZnO with other binary compounds in a quest to reduce the coercive field and/or increase the breakdown field. Wurtzite c/a lattice parameter ratio has also been used frequently to empirically predict likelihood to exhibit ferroelectricity for wurtzites, as the relationship between coercive field and c/a lattice parameter ratio was noted for $Al_{1-x}Sc_xN$ in the original Fichtner paper.[1] One way of looking at this is to treat smaller c/a values as indicative of lower energy differences between the ground state polar and the intermediate nonpolar structures. The empirical rule works well for $Al_{1-x}Sc_xN$ alloys as shown in Fig. 9(a); the measured coercive field decreases linearly with increasing Sc composition, and the wurtzite c/a values also decrease accordingly.[1,50] Recent computational studies based on NEB methods also showed that the predicted switching barrier has the same general trend with Sc composition.[39,41,45] However, the general applicability of this

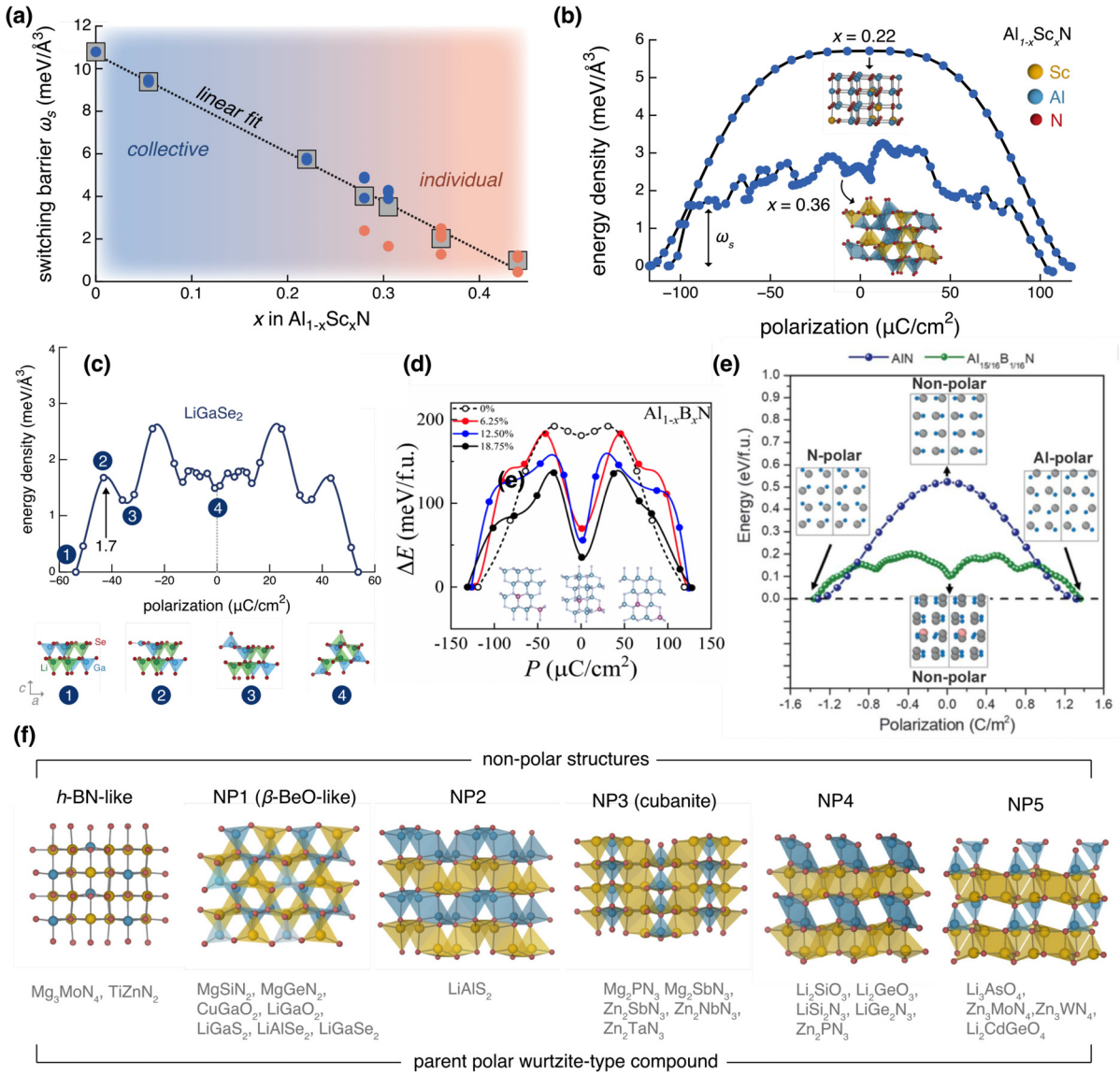

FIG. 8. (a) SS-NEB predicted switching mechanism and barrier in $Al_{1-x}Sc_xN$ alloys. (b) Two representative polarization inversion pathways for $Al_{1-x}Sc_xN$ alloys. Reproduced with permission from Lee *et al.*, Adv. Sci. **10**, eadl0848 (2024).[39] Copyright 2024 Authors, licensed under a Creative Commons Attribution (CC-BY-NC) license. (c) Polarization inversion pathway for $LiGaSe_2$ (space group $Pna2_1$) and the associated atomic structures. Reproduced with permission from Lee *et al.*, Matter **7**, 1644–1659 (2024).[40] Copyright 2024 Elsevier. (d) Polarization inversion pathway determined using the NEB method for wurtzite $Al_{1-x}B_xN$ alloys and the associated polar and nonpolar structures. Reproduced with permission from Liu *et al.*, Appl. Phys. Lett. **122**, 122901 (2023).[41] Copyright 2023 AIP Publishing LLC. (e) Polarization inversion pathway determined using the NEB method for wurtzite $Al_{1-x}B_xN$ alloys and the associated polar and nonpolar structures. Reproduced with permission from Calderon *et al.*, Science **380**, 1034–1038 (2023).[30] Copyright 2023 The American Association for the Advancement of Science. (f) Nonpolar structures identified among studied multinary wurtzite-type compounds. Reproduced with permission from Lee *et al.*, Adv. Sci. **10**, eadl0848 (2024).[39] Copyright 2024 Authors, licensed under a Creative Commons Attribution (CC-BY-NC) license.

concept remains limited to trends within individual alloys and fails to capture relationships across alloy families, such as when comparing $Ga_{1-x}Sc_xN$ to $Al_{1-x}Sc_xN$.

Recently, Yazawa *et al.* showed that ferroelectric behavior in wurtzite nitrides depends on local chemical environment rather than extended structural parameters such as c/a ratio.[50] Their DFT calculations showed that the composition-dependent change in ferroelectric response is dominated by the more ionic nature of the Sc–N bonds and the resulting local distortions of the neighboring Al–N bonds. The change in wurtzite c/a is not the *cause* of a reduced E_c, but both are consequences of a change in local bond ionicity. Lee *et al.* extended this conclusion to a larger chemical space and found that wurtzite c/a lattice parameter ratio has no correlation with polarization switching barrier across different chemistries [Fig. 9(a)[40]]. Higher bond ionicity

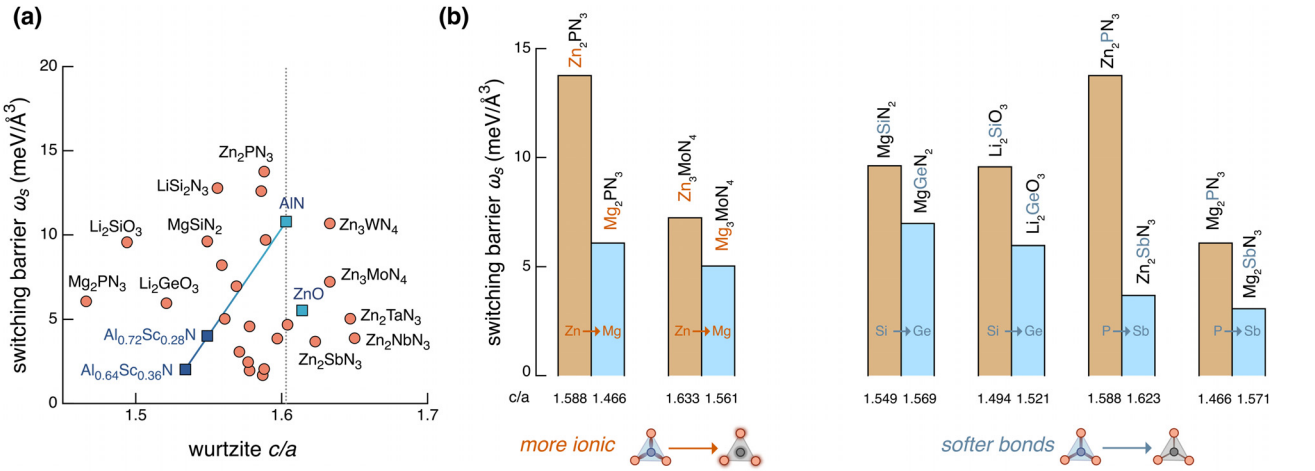

FIG. 9. (a) Wurtzite c/a lattice parameter ratio has no correlation with polarization switching barrier across different chemistries. (b) Bond ionicity and softness are two qualitative design principles that do directly impact switching barrier. Reproduced with permission from Lee *et al.*, Matter **7**, 1644–1659 (2024).[40] Copyright 2024 Elsevier.

and softer bonds consistently lead to lower polarization switching barriers as shown in Fig. 9(b). More recent work from Jia *et al.* reveals similar structural factors in (Zn,Mg)O, though it focuses on the piezoelectric rather than ferroelectric response.[51]

Thus, a more general approach to understanding coercive fields and polarization reversal in wurtzites is called for. The polarization switching barrier in the case of the $wz^+ \rightarrow hex^0 \rightarrow wz^-$ (see Fig. 4) inversion pathway is essentially the energy difference between a polar wurtzite and the corresponding nonpolar layered hexagonal structure (both structures share the same cell size and shape). Moriwake *et al.* performed a computational search among MX binary wurtzites (M = Zn and Be, X = O, S, Se, and Te) in 2014[22] to identify wurtzites with sufficiently low switching barriers that polarization inversion may be feasible. They later expanded the MX binary wurtzite search space to include SiC, pnictogenides (M = Al, Ga, and In), chalcogenides (M = Be, Mg, Mn, Zn, and Cd), and halides (M = Cu and Ag) excluding fluorine [see Fig. 10(a)].[52] The polarization switching barrier was reported to decrease with decreasing ionic radius ratio (r_{anion}/r_{cation}). Moriwake *et al.* correlated the trend with stability of cation–anion tetrahedra,[52] but the trend can be also understood in terms of the design principles from Lee *et al.* and Yawaza *et al.* that higher bond ionicity leads to lower switching barrier.[40,50] For the same anion group, e.g., pnictogens, the more electronegative element has a smaller anionic radius and forms more ionic bonds with a given cation than the less electronegative one. Similar computational approaches have also suggested ferroelectricity in Mg_2XN_3 (X = Sb, Ta, Bi, Nb, V, and Cr), with large spontaneous polarization ($\gtrsim 80\,\mu C/cm^2$) and switching barriers (>0.85 eV/f.u.) predicted.[53,54]

First-principles studies on YN and LaN have found that wurtzite and rock salt LaN have comparable formation enthalpies,[46] consistent with previous syntheses of LaN,[55,56] and that wurtzite LaN has a lower switching barrier (0.06 eV/f.u.) than $Al_{0.8}Sc_{0.2}N$ (0.12 eV/f.u.).[45] Experimental confirmation is still needed, and it should also be noted that wurtzite LaN has significantly lower bandgap (~2.3 eV) than AlN (~6.0 eV).[46]

Calculations are of course not limited to thermodynamically stable materials. For example, Dai and Wu built upon the insight that ionic salts, which generally prefer rock salt or CsCl structures, might exhibit much lower switching barriers than AlN or ZnO-based materials if stabilized in the wurtzite structure.[44] The trends are consistent with the ionicity arguments already noted.

Energy barriers to switching are only half of the challenge to discovering new ferroelectrics, however, as the material must be able to withstand the necessary electric field to overcome these barriers. Prediction of defect-driven catastrophic dielectric breakdown is infeasible (and somewhat irrelevant) for materials search purpose, but intrinsic electronic breakdown can be estimated as a proxy for the maximum electric field that might be applied to an ideal material. Based upon one such phenomenological model that depends on maximal phonon frequency at the Γ point and electronic bandgap[57] and using AlN as a reference, Lee *et al.* suggested four candidate materials (Li_2GeO_3, Li_2SiO_3, $MgSiN_2$, and Mg_2PN_3) that are predicted to have both higher breakdown fields and lower switching barriers than AlN [Fig. 10(c)].[40,58] Including comparable results for $Al_{1-x}Sc_xN$ alloys on the same figure[39] shows how alloying can decrease switching barrier more rapidly than intrinsic breakdown field and enables a notional extrapolation for alloying other compounds.

Lee *et al.* further showed that the calculated switching barriers are associated with the more-electronegative cations in all studied multinary compounds and alloys. This suggests that alloying with more electropositive cations should increase the bond ionicity and reduce switching barriers.[39] Subsequent independent reports of Sc-substituted $LiGaO_2$ by Yasuhara *et al.*[59] and (Al,Gd)N[38] are consistent with this design principle.

III. IMPLICATIONS ON ELECTRICAL RESPONSE OF WURTZITE FERROELECTRICS

The electrical (and related) properties make ferroelectrics of interest for integrated devices. Thus, it is valuable to cover the electrical characteristics and behaviors of wurtzite ferroelectrics, particularly when (and why) they may differ from the responses of more well-known ferroelectrics.

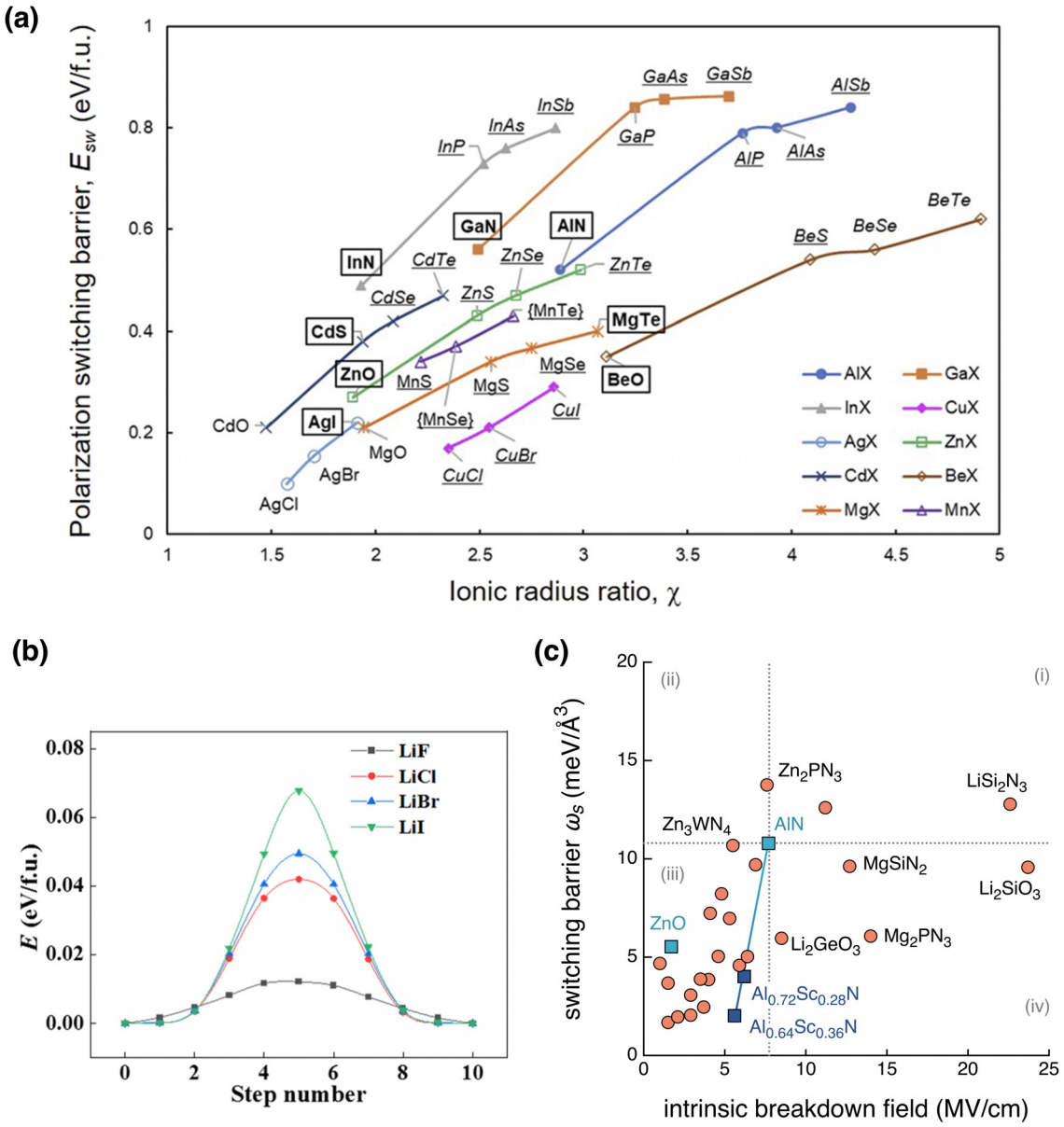

FIG. 10. (a) Predicted polarization switching barrier as a function of ionic radius ratio (r_{anion}/r_{cation}) for binary wurtzites. Reproduced with permission from Moriwake *et al.*, APL Mater. **8**, 121102 (2020).[52] Copyright 2020 Authors, licensed under a Creative Commons Attribution (CC BY 4.0) license. (b) Polarization switching barrier of binary wurtzite salts. Reproduced with permission from Dai and Wu, Sci. Adv. **9**, eadf8706 (2023).[44] Copyright 2023 Authors, licensed under the Creative Commons Attribution (CC-BY-NC) license. (c) Polarization switching barrier and intrinsic breakdown field for wurtzite-type multinary compounds. Reproduced with permission from Lee *et al.*, Matter **7**, 1644–1659 (2024).[40] Copyright 2024 Elsevier.

A. Loop shape

We begin by tracing out a ferroelectric hysteresis loop. When a gradually-increasing electric field is applied to any ferroelectric, the change in polarization is (roughly) linear—proportional to the relative permittivity—until the field is sufficient to begin reorienting spontaneous dipoles, beyond which the measured polarization will be a superposition of the induced polarization and reoriented spontaneous dipoles until all of the spontaneous dipoles are as aligned as they can be and the sample saturates. In polycrystalline ceramics such as soft Pb $(Zr,Ti)O_3$ (PZT) compositions, this poling process can be quite gradual because the field projection onto different polarization directions across different grains leads to a broad distribution in effective local coercive fields. The reversal process will have a narrower distribution of starting polarization directions and therefore a less-gradual

transition. For uniaxial single crystals, the distribution of starting polarization states is narrower, so the hysteresis loop shape is more square; for uniaxial crystals, polarization rotation is presumed zero, further sharpening the loop squareness.

Thus, given the large value and single-axis P_S of the wurtzite structure and the large coercive fields, it is perhaps not surprising that the measured loops for ferroelectric wurtzites look different from those typical for PZT, but the differences even from $LiTaO_3$ loops are striking (Fig. 11).[60] Of course, the axes of P vs E plots do not explicitly include a time component, but all reputable wurtzite hysteresis loops reported to date—measured across more than 6 orders of magnitude of frequency, different chemistries, temperatures, geometries, and stress states—show loops that are much more square than is typical for other ferroelectrics. Such abrupt reversal justifies a closer look at the kinetics of switching.

B. Kinetics

The fundamentals of ferroelectric switching kinetics have been extensively investigated over the past century. A very important step in this direction was the application of general nucleation and growth kinetics[61–65] to ferroelectric switching by Ishibashi in 1971. This leads to the formulation of what is now known as the Kolmogorov–Avrami–Ishibashi (KAI) model,[66]

$$f = 1 - \exp\left[-(t/t_0)^n\right], \tag{4}$$

where f is the volume fraction switched at time t, t_0 is the characteristic time, and n is the Avrami exponent. The Avrami exponent corresponds to the domain growth dimensionality, D, when switching is dominated by growth of existing nuclei, or $1 + D$ when there is a constant nucleation rate that occurs simultaneously with growth.[66,67] Thus, under the Ishibashi boundary conditions—which, crucially, assume the presence of preexisting nuclei—the possible range of Avrami exponent is $1 < n < 4$.

Tagantsev *et al.* rationalized $n < 1$ with the introduction of a nucleation limited switching (NLS) model,[68] which is governed by nucleation time distribution with no significant domain growth. This model can describe, among other possible scenarios, a distribution of coercive fields due to a distribution of crystallographic orientations.[68] The NLS model has been successfully applied to the kinetics of polycrystalline ferroelectric thin films such as PZT and HfO_2-based materials.[69,70]

Wurtzite ferroelectric $Al_{0.64}Sc_{0.36}N$ follows the KAI model for the switching time window $> 10^{-4}$ s.[71] However, at the faster switching time window $< 10^{-5}$ s, the Avrami exponents of $Al_{0.7}Sc_{0.3}N$ and $Al_{0.94}B_{0.06}N$ significantly exceed the physically rational range $n > 4$.[60] One reasonable scenario is that significant domain growth occurs simultaneously with an increasing nucleation rate, a scenario not captured under Ishibashi's assumed starting conditions. This scenario has been labeled the simultaneous non-linear nucleation and growth (SNNG) model.[72]

This model rationally describes the abrupt ferroelectric switching kinetics seen in the $Al_{0.7}Sc_{0.3}N$ and $Al_{0.94}B_{0.06}N$ films as seen in Figs. 12(a) and 12(b). The colored dots are experimental results, and black lines are simulated curves based on the SNNG equation. The SNNG fitting was conducted for polarization evolution, which was directly obtained from the switching current transient. The significant domain growth corresponding to the peak switching current [$\sim \bar{t}_{imp}$, average impingement time, as shown in Figs. 12(c) and 12(d)] is faster than the simulated nucleation rate peak time [τ_{peak} as shown in Figs. 12(e) and 12(f)] at high electric fields, which indicates that simultaneous non-linear nucleation and growth occur. Note that this growth-nucleation relationship does not imply that growth of an individual domain occurs before nucleation of the same domain (which would be non-physical); instead, this shows that the early nuclei exhibit significant growth while the rate of additional nucleation is still increasing. It is this non-negligible growth *prior to the peak in nucleation rate* that is not captured in the classic KAI model, which explicitly assumes a population of preexisting nuclei.[60] The non-linear nucleation rate and the simultaneous nucleation-growth were verified with direct domain observation via a piezoelectric force microscopy (PFM) technique [Fig. 12(g)].[72] Note that the SNNG model also covers the kinetics at $\tau_{peak} < \bar{t}_{imp}$ observed at lower electric field for the materials; in other words, when the situation matches Ishibashi's originally assumed boundary conditions, the SNNG model collapses to full equivalence with the traditional KAI model (Fig. 13).

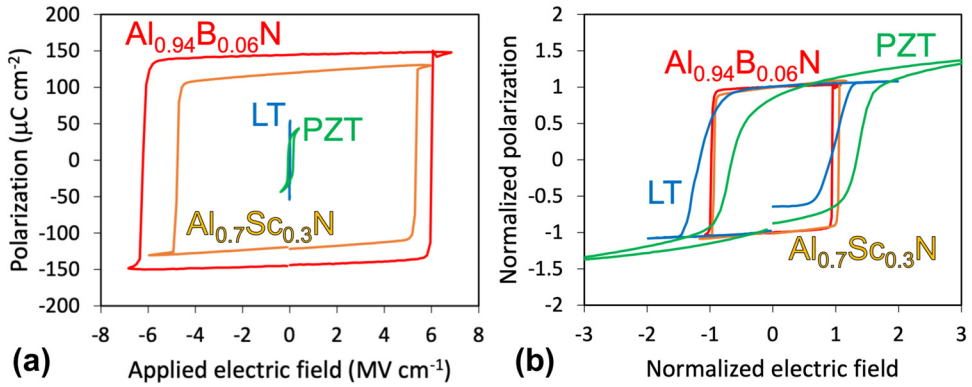

FIG. 11. Wurtzite-structured nitride ferroelectrics exhibit hysteresis loops that are far more square than those of prototype ferroelectrics such as single crystal $LiTaO_3$ (LT) and thin film $PbZr_{0.52}Ti_{0.48}O_3$ (PZT). For clarity of comparison, (a) shows directly measured data and (b) shows the same data with both P_r and E_c normalized. Reproduced with permission from Yazawa *et al.*, Mater. Horiz. **10**, 2936 (2023).[60] Copyright 2023 Authors, licensed under a Creative Commons Attribution (CC BY 3.0) license.

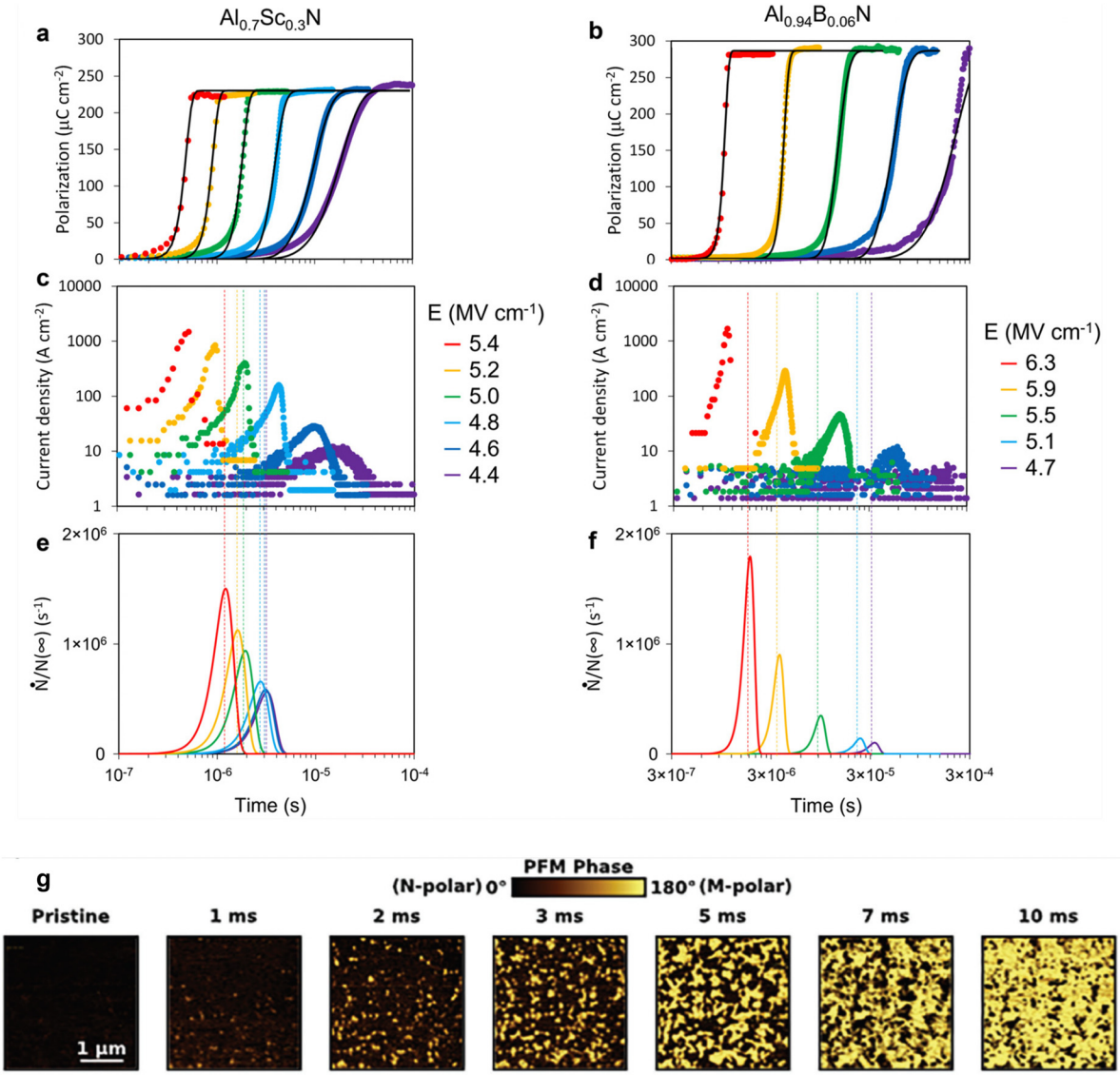

FIG. 12. Evolution of switched polarization under various driving electric fields. (a) Electric field dependence of the polarization vs time curves for $Al_{0.7}Sc_{0.3}N$ and (b) for $Al_{0.94}B_{0.06}N$. Colored data points in the polarization–time curves represent measured data; black lines represent simulated results using the SNNG model. Switching current vs time curve for (c) $Al_{0.7}Sc_{0.3}N$ and (d) for $Al_{0.94}B_{0.06}N$. Normalized nucleation rate curves used for the simulation for (e) $Al_{0.7}Sc_{0.3}N$ and (f) $Al_{0.94}B_{0.06}N$. Reproduced with permission from Yazawa *et al.*, Mater. Horiz. **10**, 2936 (2023).[60] Copyright 2023 Authors, licensed under a Creative Commons Attribution (CC BY 3.0) license. (g) PFM phase image for direct observation of number of nucleation site and growth evolution for $Al_{0.85}Sc_{0.15}N$. Reproduced with permission from Guido *et al.*, Adv. Sci. **11**, 2308797 (2024).[72] Copyright 2024 Authors, licensed under a Creative Commons Attribution (CC BY 4.0) license.

C. Wake-up, nucleation, and partial switching

The complexity of polarization reversal in wurtzites does not end with understanding the kinetics of a single reversal cycle: wake-up and fatigue phenomena have also been reported and will be crucial for eventual device deployment—especially in the context of memory applications.

Wake-up refers to a gradual increase in switchable polarization with an increasing number of switching cycles, and fatigue refers to a degradation in switching performance with increased cycle number that is commonly associated with end-of-life from a device performance perspective. Fatigue typically manifests as a gradual decrease in switchable polarization, but occasionally the term is used to describe a gradual loss in resistivity that results in leakage currents dominating over switching currents. Both terms are phenomenological in origin, deriving from a device perspective (e.g., memory) to describe suitability for operation rather than underlying mechanisms. Both have been studied in perovskite oxide ferroelectrics[73–76] as well as in HfO_2-based films.[77–79]

Reports of wake-up requirements in wurtzite ferroelectrics vary widely,[35,80–85] and interpretation is further complicated by the large number of papers that simply do not describe the presence or absence of a wake-up procedure in detail. An important early study on sputter-deposited $Al_{0.93}B_{0.07}N$ films woken-up over the course of about 40 cycles of 6 MV cm^{-1} 100 Hz triangular excitation [Fig. 14(a)][80] proposed that the origin of wake-up behavior is a gradual increase in the density of mobile domain walls, based on the measured increase in the reversible Rayleigh coefficient with cycling [Fig. 14(b)]. The gradual increase in the number of nuclei of antiparallel domains with cycles is schematically illustrated in Fig. 14(c); it is this increase that was proposed to gradually facilitate ferroelectric switching.

A subsequent investigation into the origin(s) of wake-up and domain wall dynamics in an $Al_{0.94}B_{0.06}N$ film measured the cycle dependence of switching kinetics measured under positive-up-negative-down (PUND) pulse trains and combined these data with measured piezoelectric response after each cycle (Fig. 15) and post-cycle etching.[81] Significant asymmetric switching speeds were observed: polarization switching from nitrogen polar to metal polar is slower than the other direction as shown in Fig. 15(a). In addition, the time required to transition from nitrogen polar to metal polar under the same conditions decreases with cycling, which corresponds to the decreased coercive field with cycles that leads to the observed wake-up behavior.

Measurements of the piezoelectric coefficient ($d_{33,eff}$) allows quantification of domain volume information because the measured value of ($d_{33,eff}$) is directly reduced by the volume of antiparallel domains under test (it is worth remembering that such piezoelectric and polarization reversal measurements typically involve several percent uncertainty). For the state before transition from nitrogen polar to metal polar (before the N pulse in the PUND sequence), a slight decrease in measured $d_{33,eff}$ with increasing the cycle is seen, consistent with an increase in antiparallel domain mixture during the wake-up cycles [Figs. 15(b) and 15(c)]. This result is consistent with the Rayleigh behavior shown in Fig. 14(b). The accompanying reduction in piezoelectric coefficient before the P pulse is also consistent with a significant parallel/anti-parallel domain mixture, although the significantly faster metal-to-nitrogen switching process means that this pre-P pulse mixed state situation does not contribute significantly to the wake-up behavior.

It is also worth noting that some studies[80,81] have noted that the etching process seems to be "cleaner" for films following cycling and/or wake-up, suggesting that switching is more complete after wake-up. This would be consistent with the observation of IDBs in as-grown films[86] on GaN but would seem to contradict the Rayleigh results mentioned earlier [Fig. 14(b)]. Such interpretations might be reconciled by remembering that Rayleigh behavior is a measure of *mobile* interfaces, so if as-grown IDBs are very strongly pinned, they would not contribute to a measured Rayleigh response but could still impact chemical etching. Furthermore, if the total antiparallel volume associated with IDBs is within the uncertainty of macroscopic electrical and electromechanical measurements, their presence or absence could easily be overlooked. However, even a small volume of antiparallel domains could make a big difference in the surface following chemical etching. Thus, the "cleaner" etching results observed after wake-up would be consistent with the earlier arguments if the switching associated with wake-up overtakes a non-zero population of IDBs present during growth.

Importantly, wake-up behavior depends on measurement conditions. The number of cycles required to wake-up decreases with increased applied electric field amplitude [Figs. 16(a) and 16(b)],[87] higher measurement temperature [Fig. 16(c)], and lower measurement frequency [Fig. 16(d)].[83] The activation energy for the wake-up process is ~0.15 eV, which is roughly 5× larger than that of the switching process (~0.028 eV[88]). This indicates that the initial nucleation is more energy consuming than domain growth, which is in good agreement with the nucleation delay associated with the large nucleation barrier discussed by Yazawa *et al.*[60] In spite of some wurtzite ferroelectric thin films usually showing wake-up during their initial switching cycles, $Al_{1-x}Sc_xN$ films have also been described as wake-up free, as a saturated polarization can be recovered through the first switching event with variance in subsequent coercive field values being in the low single-digit % range. Thus, whether or not wake-up is observed in wurtzite ferroelectric films depends at least as much on the growth and

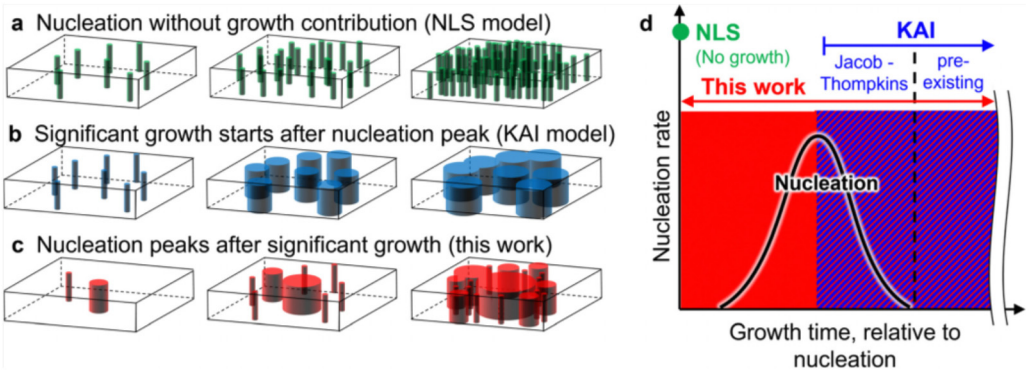

FIG. 13. Ferroelectric switching process according to (a) nucleation-limited switching (NLS) with no significant domain growth, (b) the KAI model in which nucleation can be described by a population of preexisting nuclei and/or a (Jacob-Thompkins) decreasing nucleation rate followed by growth and impingement. (c) Simultaneous non-linear nucleation and growth model including scenarios in which nucleation rate peaks significantly after the onset of growth. This is done by (d) describing all nucleation processes according to a power law distribution and relaxing the assumptions that restrict the KAI model to specific cases in which nucleation rate peaks prior to the onset of significant growth. Reproduced with permission from Yazawa *et al.*, Mater. Horiz. **10**, 2936 (2023).[60] Copyright 2023 Authors, licensed under a Creative Commons Attribution (CC BY 3.0) license.

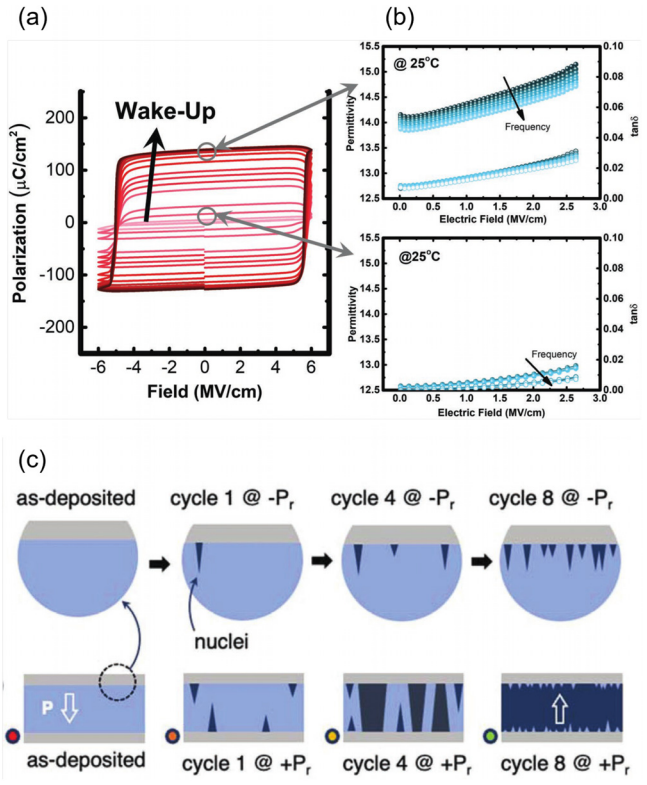

FIG. 14. Many wurtzite ferroelectrics exhibit some form of wake-up. Zhu *et al.*[80] described (a) the cycle-dependent increase in switchable polarization and its (b) related effect on Rayleigh response. They also (c) proposed a conceptual model of domain evolution in such films. Reproduced with permission from Zhu *et al.*, Adv. Electr. Mater. **8**, 2100931 (2022).[80] Copyright 2022 John Wiley and Sons.

affiliated interfaces and defects of the sample as well as the measurement conditions than on the intrinsic structure or chemistry. Unlike in fluorite type ferroelectrics, there is currently no evidence that the wake-up process in wurtzite ferroelectrics is accompanied by major structural changes. Thus, the spontaneous polarization is not really increased even under conditions where wake-up is observed, but rather *switchability is enhanced*, suggesting a domain nucleation-growth origin.

Fatigue is also commonly observed but relatively rarely reported in wurtzite ferroelectrics.[83–85,89] One study associated the reduction in switchable polarization in (Al,B)N with a reduction in electrode area from extrinsic breakdown damage, indicating that the low fatigue endurance reported so far (in this case, $\sim 10^6$ cycles) is not limited by intrinsic degradation of the actual ferroelectric material during cycling [Figs. 16(c) and 16(d)]. Oxygen impurities have also been suggested as an origin of fatigue behavior after even fewer cycles ($\sim 10^3$) in some (Al,Sc)N films, as fatigue endurance was shown to improve by orders of magnitude by annealing under a reducing atmosphere (H_2 or NH_3).[84,85]

IV. APPLICATIONS OF POLARIZATION DOMAINS IN WURTZITE FERROELECTRICS

Due to their outstanding properties such as a wide and tunable bandgap and high spontaneous polarization, wurtzite III-N materials found successful application in optical (e.g., light emitting diode—LED) as well as in power electronic (e.g., HEMT) devices. For instance, the discontinuity of the spontaneous polarization between (usually) AlGaN and GaN gives rise to the formation of the two dimensional electron gas (2DEG), the channel of the HEMT. The 2DEG features a higher charge carrier velocity and mobility compared to traditional Si-based transistors.[90] Together with the high bandgap of GaN, this makes HEMTs promising candidates for next-generation energy efficient power radio frequency (RF) devices suitable for a broad spectrum of applications ranging from wireless communication to automotive, industry, and information technology.[91–93]

The wurtzite-type III-N ferroelectrics such as $Al_{1-x}Sc_xN$ share the general properties of wurzite III-N materials and exhibit—compared to other ferroelectrics—a relatively low dielectric constant and dielectric loss combined with a moderate piezoelectric response.[94,95] $Al_{1-x}Sc_xN$ has become well-established in industry for piezoelectric applications as for example, the active layer in-state-of-the-art radio frequency (RF) filters.[96,97] With the realization that these same materials can be ferroelectric, polarization switching of the active layers in these already well-established devices is in principle accessible and the polarization direction is no longer solely determined by growth. Thus, ferroelectric switching can be exploited to extend the functionality of these devices without the need to introduce a new material into

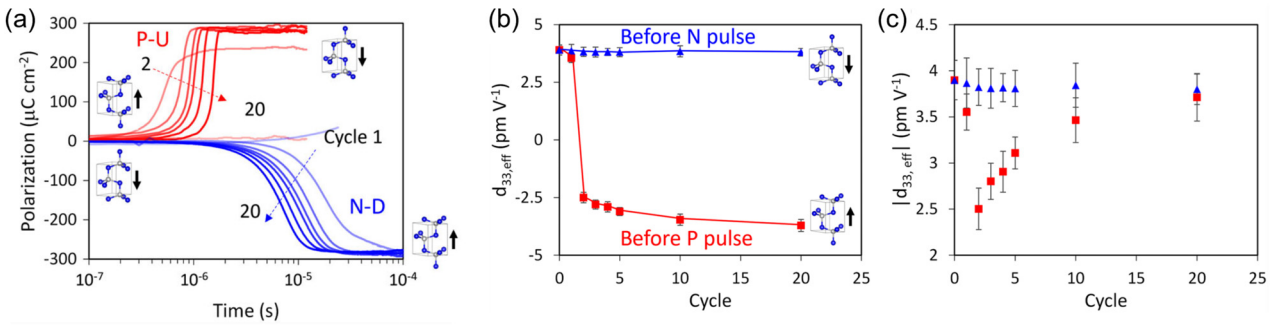

FIG. 15. Wake-up is asymmetric (polarity-dependent) in both (a) the time-dependence of polarity inversion and evolution of this time-dependence with cycling. Evolution (b) and (c) of piezoelectric response with cycling is also asymmetric. Reproduced with permission from Yazawa *et al.*, J. Am. Ceram. Soc. **107**, 1523–1532 (2023).[81] Copyright 2023 John Wiley and Sons.

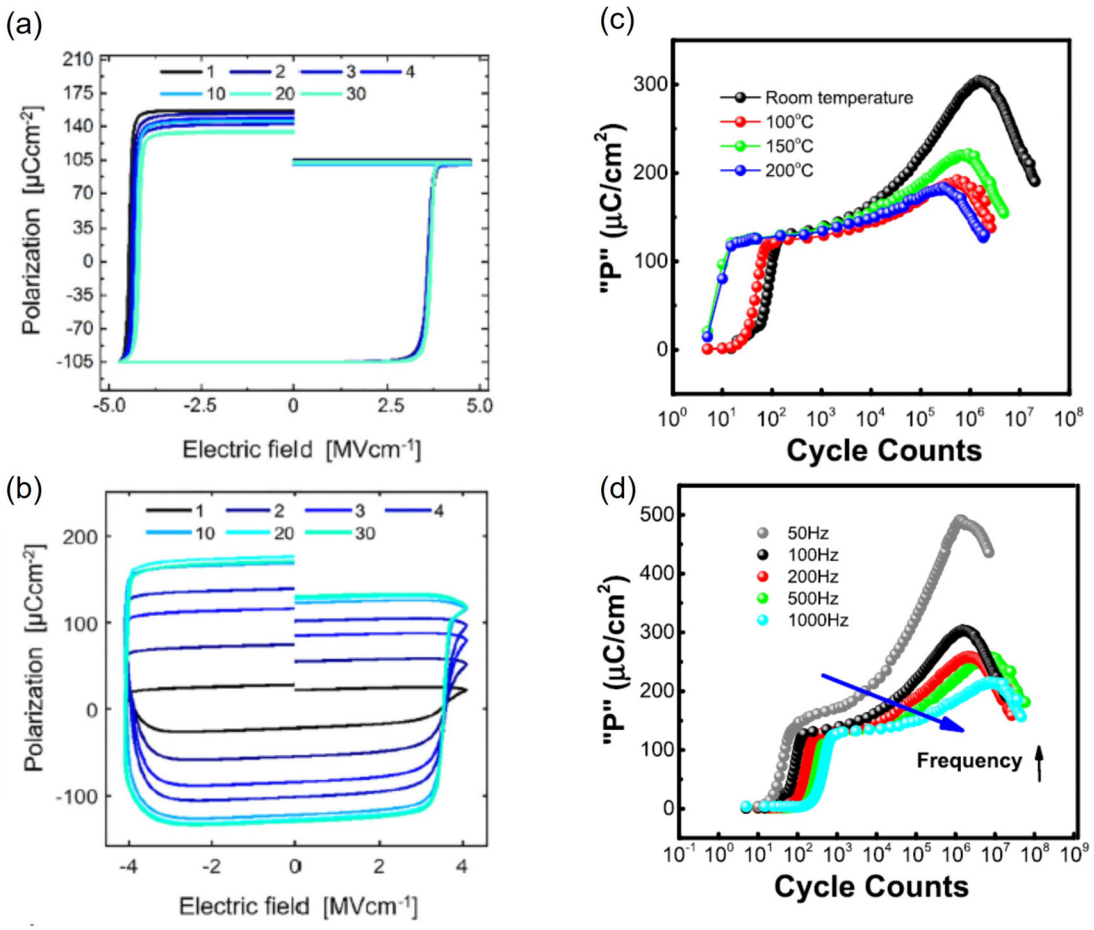

FIG. 16. One of the reasons for apparent inconsistencies across literature reports of wake-up behavior in wurtzite ferroelectrics may be (a) and (b) the strong dependence of wake-up on measurement conditions relative to coercive field, which itself varies with cycle and frequency. Depending on, e.g., the applied electric field amplitude, a film might appear to undergo strong wake-up or, for a slightly larger field, be wake-up free. Reproduced with permission from Gremmel and Fichtner, J. Appl. Phys. **135**, 204101 (2024).[87] Copyright 2024 Authors, licensed under a Creative Commons Attribution (CC BY 4.0) license. (c) and (d) Fatigue in current generation wurtzite ferroelectrics also seems to be dominated by extrinsic (e.g., defects, interfaces, and breakdown) effects rather than representing any sort of inherent material limitation to switching endurance. Reproduced with permission from He *et al.*, Acta Mater. **266**, 119678 (2024).[83] Copyright 2024 Authors, licensed under a Creative Commons Attribution (CC BY-NC-ND) license.

the layer stacks. Consequently, dynamic polarization tuning of HEMTs[98–100] and dynamic frequency and transmission level adjustments in RF filters[101] have been reported recently,[102] in addition to more classical ferroelectric memories such as FeFETs and tunnel junctions. In the following, we provide an overview of potential applications that aim to harness the ferroelectric properties of the wurtzite structure.

A. Memory

The emergence of ferroelectricity in wurtzite-type ferroelectrics sparked interest in their integration to nonvolatile memory in a number of different architectures. In addition to the comparably low power consumption and fast access and write times of ferroelectric memories in general, the large E_c and P_r values of wurtzite-type ferroelectrics promise long retention times and distinct states even with aggressive scaling. Retention times of >10 years have been extrapolated, and outstanding stability under H_2 post-treatments up to 600 °C and anneals up to at least 1100 °C has been reported.[89,103–105] Thus, all-nitride and SiC-based heterostructures are being studied for memory applications under harsh environments. Full epitaxial integration of wurtzite-type ferroelectrics with III–V platforms has been demonstrated.[37,86,106–109] Sputter-deposition of AlN-based materials is already well-established and scaled, so the demonstrated thickness scalability of $Al_{1-x}Sc_xN$ for reaching switching voltages in the range of 1 V might be rapidly transferable to existing semiconductor production equipment.[31,110]

One persistent challenge, though, is that the large electric fields required for ferroelectric switching result in large leakage currents in wurtzite-type ferroelectrics close to E_c, particularly in very thin films. Several groups have reported a superlinear increase in leakage current as film thickness is reduced in wurtzite-type ferroelectrics,[87,111–113] and this superlinearity appears to be at least partially driven by the character of the ferroelectric domain walls themselves.[31] Such leakage currents increase power consumption and reduce read/write margin; coupled with the comparably low cycling endurance demonstrated to

date (see above), this restricts immediate adoption of wurtzite-type ferroelectrics for traditional high-cycle memory applications. However, current state-of-the-art wurtzite-type ferroelectrics could be suitable already for different architectures with more modest switching cycle requirements. For example, memory cells with individual weights (e.g., resistance states) interconnected in the form of a crossbar array enable parallel multiply and accumulate (MAC) operations,[114,115] which are the basis of inference in deep neural networks (DNNs). Multi-level memory functionality additionally allows targeting of advanced neuromorphic concepts such as synaptic plasticity and integrate-and-fire functionality.

Analog-like storage of individual states as well as linear potentiation and depression have been demonstrated for an $Al_{1-x}Sc_xN$-based two-dimensional FeFET [see Figs. 17(a) and 17(b) as well as FeFETs based on standard silicon technology].[103,116] Additionally, various two-terminal $Al_{1-x}Sc_xN$-based multi-level memory devices were demonstrated in recent years.[117–121] The role of the polarization state of the ferroelectric on the current response of an example device consisting of a Ti/Au/$Al_{1-x}Sc_xN$/n-GaN capacitor stack is depicted in Fig. 17(c).[119] Individual intermediate states are addressable (i.e., memristive behavior) due to controlled partial polarization switching of the ferroelectric. In the case of the FeFET, the field effect that ultimately arises from the net polarization state of the ferroelectric layer modulates the conductivity of the channel. In the case of the two-terminal devices, (partial) polarization switching is typically related to a change of the effective barrier height at the interface, which in turn modulates the conductivity. The analog-like behavior of the 2D-FeFET suggests that the sign and magnitude of the field effect associated with the two polarization states (M-polar and N-polar) can be arbitrarily fine-tuned, at least for the device sizes that have been investigated so far.

The possibility of analog-like operation is further corroborated by the fact that nm-sized domains have been imaged in individual grains of $Al_{1-x}Sc_xN$ (Fig. 7)—instead of the grain-by-grain switching reported in scaled devices using ferroelectrics with a fluorite structure.[31,122] 2D-FeFET channel lengths and widths down to 80 and 500 nm, respectively, and thus high scalability together with back end of line (BEOL) compatibility were also demonstrated.[103] Figure 17(a) depicts the device-to-device variability of 30 devices with margins that clearly allow for 2-bit operation. Appropriate state margins and analog-like operation for wurtzite-type ferroelectrics can be expected also if the lateral device dimensions are reduced even more aggressively, whereas for HfO_2-based FeFETs grain-by-grain switching is suggested as the limiting factor in terms of scaling and multi-level memory capabilities.[122] For wurtzite-type ferroelectrics, as soon as the lateral dimensions of the device are smaller than the lateral grain size (≈ 10–30 nm for $Al_{1-x}Sc_xN$), partial polarization switching can in principle still occur through the nucleation and growth of inversion domains inside the single grain. However, definite experimental demonstration that domains can allow analog operation in devices with grain sized dimension remains open. Surprisingly, the ferroelectric response as well as the shape and lateral dimensions of polarization domains in single-crystal $Al_{1-x}Sc_xN$ grown by metalorganic chemical vapor deposition (MOCVD)/molecular beam epitaxy (MBE) (i.e., no grain boundaries) and in textured $Al_{1-x}Sc_xN$ grown by sputter deposition (i.e., highly c-axis oriented columnar grains) are rather similar,[109] which suggests that the domain dynamics are not strongly affected by the presence of grain boundaries in wurtzite-type ferroelectrics.

The FeFET concept can be generalized to non-CMOS-based devices like GaN-based HEMTs. Since their channel is formed by a 2DEG that in turn depends on a polarization discontinuity between (usually) AlGaN and GaN (although a $Al_{1-x}Sc_xN$ barrier itself can result in even higher carrier densities[123–125]) GaN-HEMT devices are normally on. Normally on devices are, however, not desirable for high power applications due to safety reasons. Here, a sufficiently large modulation of their threshold voltage through a ferroelectric gate could be an attractive approach for realizing normally off devices. Due to their large polarization and natural compatibility with wurtzite GaN, III-N based wurtzite ferroelectrics appear to be particularly well suited for this type of device. Indeed, first device demonstrations, including a transition from normally on to normally off have been reported.[98,100] However, TEM investigations of MOCVD-grown $Al_{0.85}Sc_{0.15}N$/GaN heterostructures indicate polarization pinning of $Al_{1-x}Sc_xN$ to the M-polarity of the underlying GaN in the vicinity of the interface even after ferroelectric switching.[109] Further research is required in order to

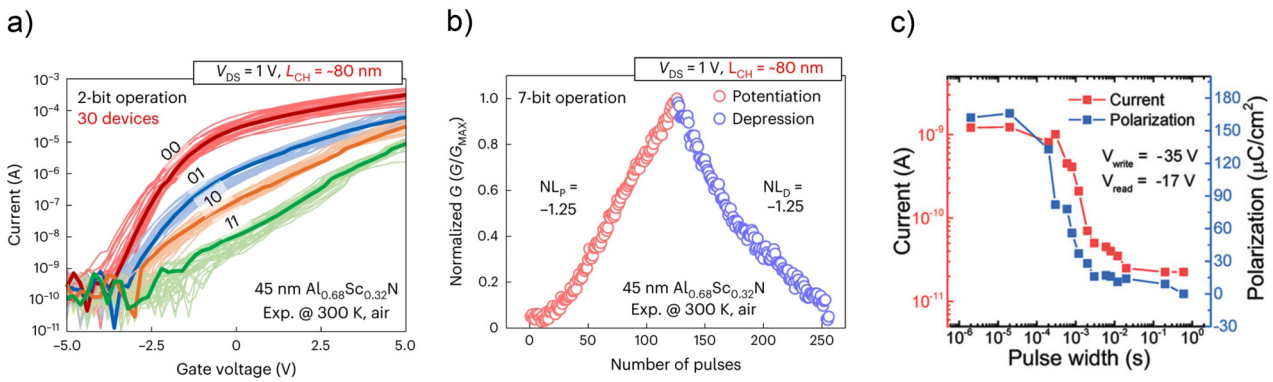

FIG. 17. (a) Multi-bit operation including device-to-device variability of 30 devices in an $Al_{0.68}Sc_{0.32}N$/two-dimensional channel ferroelectric field effect transistor. (b) Linear potentiation and depression of the same device. Reproduced with permission from Kim *et al.*, Nat. Nanotechnol. **18**, 1044–1050 (2023).[103] Copyright 2023 Springer Nature. (c) Steady-state current response and corresponding polarization state in dependence of the applied pulse width for a Au/Ti/$Al_{0.82}Sc_{0.18}N$/GaN capacitor exhibiting memristive behavior. Reproduced with permission from Wang *et al.*, Adv. Electron. Mater. **8**, 2200005 (2022).[119] Copyright 2022 Authors, licensed under a Creative Commons Attribution (CC BY-NC-ND) license.

understand if and how such pinned domains impact the overall polarization and the associated screening charges at interfaces, including increased conductivity at the domain walls.[126]

In fact, the occurrence of inclined domain walls in $Al_{0.74}Sc_{0.26}N$ imaged via TEM was linked to increased steady-state conductivity at fields well below $E_c/2$.[31] The symmetric current response and the gradual decrease in the conductivity when partially switching from a multidomain state into a single domain state (i.e., decreasing the domain wall density) are consistent with domain wall conductivity [see Fig. 18(e)].

PFM studies on the same $Pt/Al_{0.72}Sc_{0.28}N/Pt$ capacitor stack demonstrate the clear correlation of domain wall density and increased steady-state conductivity, as depicted in Figs. 18(a) and 18(d).[127] Similarly to previously reported domain wall based memristive devices,[19,128,129] when starting from a unipolar state (either M- or N-polar), the conductivity is low. Increasing the domain wall density via partial switching results in an increase in conductivity before reaching a maximum, which is then followed by a decrease in the conductivity. These memristive devices thus feature accumulative switching that differs substantially from most other approaches for resistive switching, thereby enriching the available toolbox of memristive devices. As the concept of domain wall conductivity can have similarities to the formation of a 2DEG and metallic-like conductivity at domain walls has been reported, domain wall-based memristive devices promise high on currents and high on/off ratios.[130,131] Compared to ferroelectric tunnel junctions, this high on current density could lead to better device scalability toward smaller technology nodes.

The domain wall width of ferroelectrics is typically in the range of 1 nm, which would allow aggressive lateral scaling of such devices. The observed in-grain switching and the presence of inclined conductive domain walls in $Al_{1-x}Sc_xN$ opens the possibility of various device concepts based around domain wall conductivity.[132] However, in thin devices with high domain wall densities, it is possible that domain wall pinning could result in permanently increased conductivity, which would impact all types of ferroelectric devices. For example, in three-terminal devices such as FeFETs and FeHEMTs, this could result in increased gate leakage. While domain wall conduction for wurtzite-type ferroelectrics was observed up until now to appear only in sputter-deposited $Al_{1-x}Sc_xN$ and was lately also suggested for MOCVD-grown single-crystal $Al_{1-x}Sc_xN$,[109] it is not yet clear if it is a general effect occurring in all wurtzite-type ferroelectrics. Furthermore, the polarity of the seed layer was demonstrated to affect the type of the domain wall, e.g., for $Al_{1-x}Sc_xN$ grown on M-polar GaN head-to-head domains were observed, while for films grown on non-polar electrodes solely tail-to-tail walls were observed.[109] Structurally, the domain size and shape were demonstrated to be very similar for both configurations, although the screening charges need to be negative for head-to-head and positive for tail-to-tail walls. At present, it is not clear if and how both types differ in terms of conductivity and retention. Retention in the case of domain wall conduction-based devices not only concerns the change in polarization state (i.e., a change in volume of the individual domains), but also the retention of the domain wall conductivity itself, which could change with time, e.g., due to relaxation effects.

In all of the aforementioned devices, the memristive behavior relies on partial switching of the polarization. As discussed, due to the in-grain switching and the good thickness scalability, wurtzite-type ferroelectrics promise analog-like multi-level operation also in highly scaled (laterally and vertically) devices. Retention times of unipolar polarization states (i.e., fully M-polar or fully N-polar) were demonstrated to be well above 10 years.[103,117] However, no clear retention time extrapolations of multidomain states (e.g., a partially switched ferroelectric) are given in the literature, which could differ from the retention of the unipolar states. Among other possible considerations, memristive switching in wurtzite-type ferroelectrics involving the stabilization of domain walls inside single grains have recently been demonstrated.[31]

B. Photonics and acoustics

The control of polarization domains is also promising for photonic and acoustic resonator applications. The patterning of domains

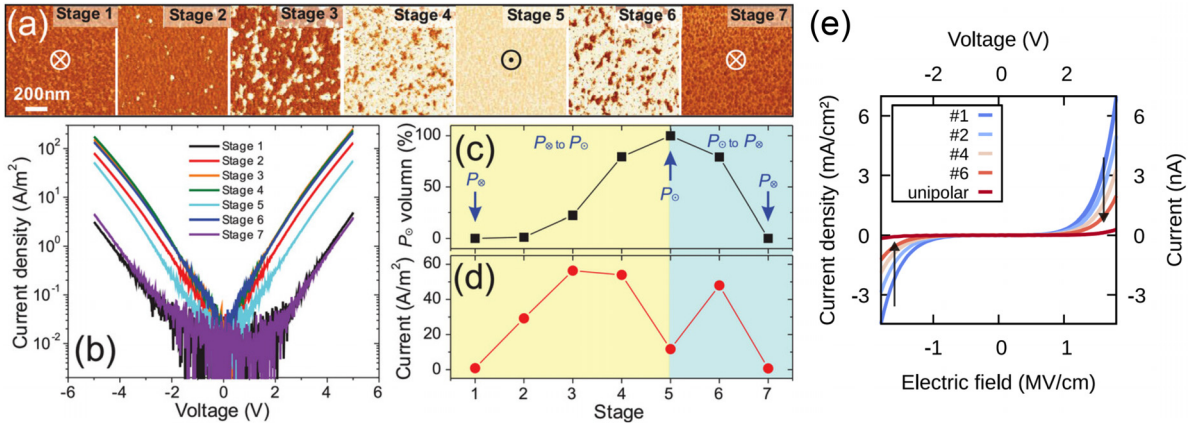

FIG. 18. (a) PFM phase images of a $Pt/Al_{0.72}Sc_{0.28}N/Pt$ capacitor switched partially into individual polarization states and (b) corresponding steady-state currents through the device. (c) Extracted area of switched polarization according to the PFM phase images and (d) the corresponding leakage current extracted at 4 V. Reproduced with permission from Lu *et al.*, Adv. Funct. Mater. **34**, 2315169 (2024).[127] Copyright 2024 Authors, licensed under a Creative Commons Attribution (CC BY-NC) license. (e) Initial measurements that demonstrate the possibility of resistive switching using domain wall conduction in $Al_{0.74}Sc_{0.26}N$—the symmetric decrease in conductivity is related to the decrease in domain wall density by gradual polarization switching. Reproduced with permission from Schönweger *et al.*, Adv. Sci. **10**, 2302296 (2023).[31] Copyright 2023 Authors, licensed under a Creative Commons Attribution (CC BY) license.

with opposite polarization direction (i.e., periodically poled structures) enables quasi-phase matching,[133] which can be used to enhance the efficiency of, e.g., second-harmonic generation (SHG).[134] In this context, the wurtzite-type ferroelectrics and in particular, $Al_{1-x}Sc_xN$ are promising due to the reported high second-order nonlinear optical susceptibility (exceeding that of $LiNbO_3$)[135] and the ability to reconfigure polarization via ferroelectric switching. To target operation toward the deep-UV regime, lateral domain sizes in the range of a few 100 nm of a periodically poled high bandgap material are required.[134] The feasibility of creating such laterally scaled structures was recently demonstrated for ferroelectric $Al_{1-x}Sc_xN$, as depicted in Fig. 19(a).[134,136]

Additionally, the alternating polarity allows manipulation of the propagation of acoustic waves, expanding function and/or design possibilities for acoustic resonators (e.g., periodically poled $LiNbO_3$, PPLN).[137,138] Ferroelectric switching in an $Al_{0.72}Sc_{0.28}N$-based Lamb-wave resonator was exploited to change the periodicity and resulted in the demonstration of dual-mode operation, as depicted in Fig. 19(b) for various pitch sizes.[139] Additionally, an $Al_{1-x}Sc_xN$-based surface acoustic wave (SAW) as well as film bulk acoustic resonator (FBAR) which could be turned on and off by ferroelectric switching was demonstrated.[101] Similar to photonics, to address high frequency operation, e.g., the X-band (8–12 GHz), a high periodicity is required for acoustic applications, as can be seen in Fig. 19(c).

Thus, the ability to create periodically poled structures in wurtzite-type ferroelectrics combined with the attractive optical and electromechanical properties makes these materials promising for next-generation functional photonic and acoustic devices. In the context of scaling, the demonstrated stable in-grain switching of lateral dimensions in the range of 5 nm highlights that in principle much higher periodicities can be achieved. Precise control of the duty cycle of the electrode array and thus precise control of the poled lateral dimensions is essential in terms of applications, e.g., in order to prevent duty-cycle errors in SHG.[140] Unintentional ferroelectric switching outside of the electrode area was demonstrated to be controllable by adjusting the poling voltage for sub-micrometer periodically poled $Al_{0.68}Sc_{0.32}N$.[134] This can in principle be used to fine-tune the duty cycle of the electrode array electrically. On the other hand, if the poling voltage is too low, the volume below the electrode will not fully invert its polarization, which in turn will disturb the periodicity.

C. Multilayer piezoelectrics

Piezoelectric actuators in the form of multilayer structures enable increased electromechanical response at low driving voltages.[141] Such structures typically consist of a number of ferroelectric layers separated by intermediate electrodes. The polarization inversion (e.g., via ferroelectric switching) of every second layer allows for interconnection of the electrodes while each layer still reacts piezoelectrically in the same manner (i.e., with contraction or expansion). Thus, the voltage required for reaching a certain displacement in a single layer can in principle be divided by the number of layers when using a multilayer structure with the same total thickness as the single layer.

While the fabrication of piezoelectric multilayer actuators using bulk ceramics is established in industry, the transfer of the concept to micro- and nanotechnology has been complicated by the fact that materials like PZT are often challenging to stabilize already as a single layer.[142] In this context, wurtzite-type piezo/ferroelectrics are advantageous due to lower deposition temperature budgets and less severe diffusion. They promise to facilitate the fabrication of such structures as the individual layers can be deposited subsequently, e.g., by sputter deposition.[143] In another study, a double-layer structure consisting of two $Al_{1-x}Sc_xN$ layers separated by a shared middle electrode where the polarization of the respective layers could be inverted individually by ferroelectric switching was demonstrated.[144] The polarity of the lower layer was ferroelectrically switched, top and bottom electrode were interconnected, and the drive voltage was applied between former and the middle electrode, see Fig. 20(a).

In Fig. 20(b), the piezoelectric response of the individual and combined layers of the multilayer structure is compared to the one of single layers with various Sc concentrations. Compared to a single layer with similar Sc concentration, an increase of 60% in $d_{33,f}$ was achieved. More recently, this was improved to $\approx 80\%$ for $x = 0.35$,[145] which however is still less than the theoretical limit of 100% increase. This is likely a consequence of pinned inversion domains present after ferroelectric switching. Their appearance is affirmed due to the decrease in $d_{33,f}$ for the lower single layer after ferroelectric switching, which implies that part of the volume is not responding or responding differently than the rest (e.g., contraction instead of expansion). Furthermore, as the spontaneous polarization in wurtzite-type materials is aligned parallel to the *c*-axes of the crystal lattice, the magnitude of the piezoelectric coefficients depend on the crystallographic texture and therefore also on the quality of the seed layer. Thus, obtaining uniform crystallographic properties for each layer can become challenging as the number of layers increases. However, the reported increase of 80% of $d_{33,f}$ is a promising initial demonstration.

V. OUTLOOK

The journey to understand the structure–property relationships in wurtzite ferroelectrics has just started. Real materials contain atomic-scale (e.g., vacancies, substitutions, inclusions, small complexes) and extended (e.g., dislocations, grain boundaries) defects that almost certainly affect the ferroelectric and dielectric properties of wurtzite-type ferroelectrics. One must, therefore, consider the existence of such defects in developing structure–property relationships. Experimental and theoretical studies so far have overlooked, perhaps not intentionally, the existence of defects and their influence on the ferroelectric properties.

Native defects are known to significantly impact the ferroelectric properties of oxide perovskites and fluorites.[146,147] For example, long-term degradation (fatigue and aging) in oxide ferroelectrics is attributed to the migration of mobile ions and oxygen vacancies.[148] Oxygen vacancies and dislocations pin domain wall motions in oxide perovskites and increase the coercive field.[149] However, due to the significant differences in bonding and ionic mobility between perovskite and fluorite oxides vs wurtzites (especially nitrides), the effects of native defects on the domain nucleation and motion as well as coercive and breakdown fields may be quite different.

First-principles studies show that nitrogen vacancies (V_N) and cation vacancies are the dominant native defects in wurtzite AlN-based alloys like $Al_{1-x}Sc_xN$ ($x \leq 0.34$) and $Al_{1-x}Gd_xN$ ($x \leq 0.25$), similar to wurtzite AlN and GaN.[150,151] In the presence of oxygen, oxygen substitutional defects (O_N) are the dominant defects.[150,151] O_N behave as DX centers—at Fermi energies closer to the conduction band, the O_N^{+1} donor captures two electrons to form O_N^{-1} acceptor. A DX center is a deep defect that forms when a donor defect like O_N^{+1} captures two electrons and undergoes a large local structural distortion

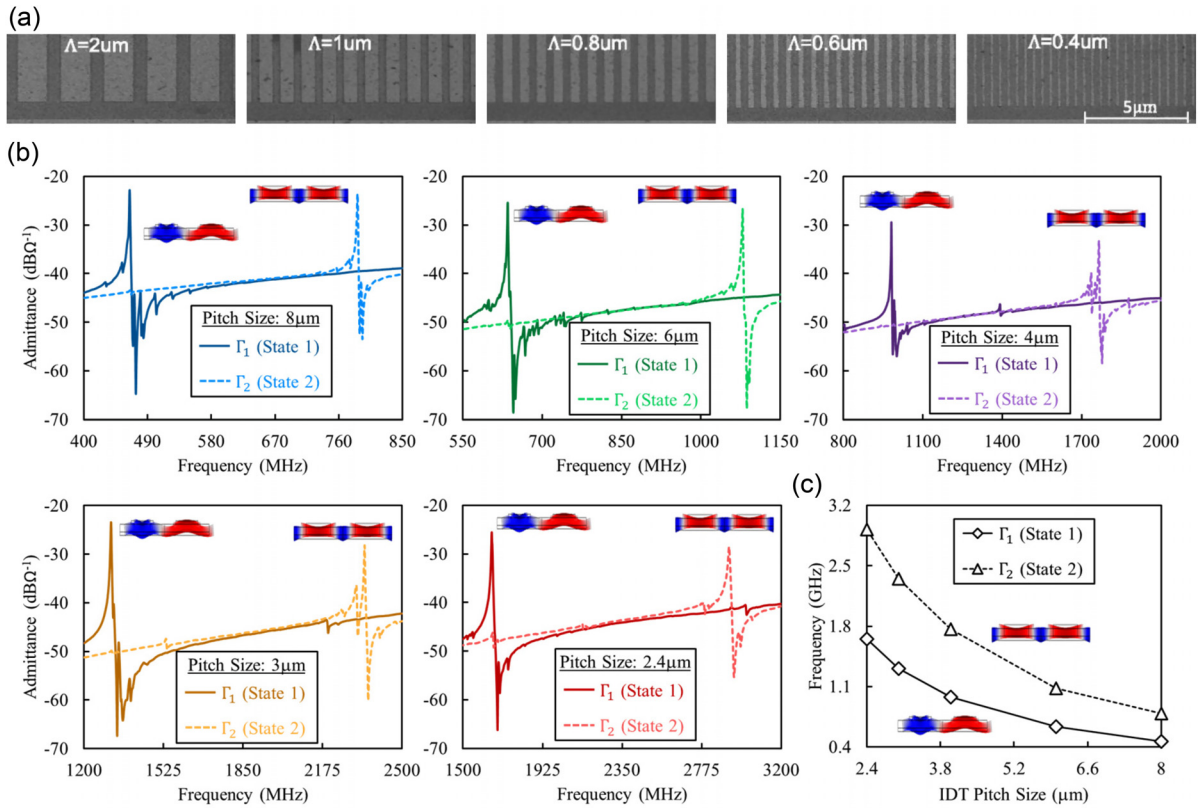

FIG. 19. (a) SEM image of periodically poled $Al_{0.75}Sc_{0.25}N$ with varying periods in the sub-micrometer regime. Prior to recording the image, the top electrodes were removed by exposure to hydrochloric acid, which also selectively etched the N-polar domains and gave rise to the contrast observed in SEM. Reproduced with permission from Yang *et al.*, Appl. Phys. Lett. **123**, 101103 (2023). Copyright 2023 AIP Publishing LLC. (b) Measured admittance of an $Al_{0.72}Sc_{0.28}N$-based Lamb-wave resonator for various interdigital transducer (IDT) pitch sizes where the resonance modes Γ1 and Γ2 are selectable by ferroelectric switching. The corresponding periodic poling is sketched in the insets. (c) The frequencies of the two operation modes depending on the IDT pitch size. Reproduced with permission from Rassay *et al.*, Micromachines **13**, 1003 (2022).[137] Copyright 2022 Authors, licensed under a Creative Commons Attribution (CC BY) license.

to stabilize an acceptor state like O_N^{-1}. Most point defects in AlN-based wide bandgap alloys exhibit multiple mid-gap states that can contribute to increased leakage currents and premature dielectric breakdown, but their concentrations can be greatly reduced through synthesis under nitrogen-rich and O-poor conditions.

However, even multi-percent levels of oxygen have been shown to *decrease* leakage in $Al_{1-x}Sc_xN$. Additionally, early computational results predict that the dominant defects such as V_N^{+1} and O_N^{+1} can reduce the polarization switching barrier at low Sc composition in $Al_{1-x}Sc_xN$.[151] This suggests that point defects can have mixed effects on wurtzite ferroelectrics, and the blanket avoidance of such defects may be not be the most effective approach. In other words, native point defects can be treated as just another substitutional defect or dopant in terms of engineering their dielectric and ferroelectric properties.

Limited evidence suggests that nitrogen vacancies (V_N) also play a critical role in fatigue and long-term breakdown, but the underlying microscopic mechanism remains elusive.[152,153] Tsai *et al.* proposed that Joule heating due to increasingly lowered Schottky barrier height is the cause of breakdown while others suggested that breakdown is caused by formation of conductive filaments of V_N.[153] The latter is similar to the established degradation mechanism in oxide ferroelectrics, but it should be noted that the bulk migration barrier of V_N (≈ 2.5 eV) is dramatically higher than that of V_O (≈ 1.0 eV) based on first-principles calculations.[154,155]

Several experimental studies have also shown rather convincingly that non-stoichiometric substitutions such as O_N,[156] Si_{Al},[157] and $(Mg_{0.5}Nb_{0.5})_{Al}$[158] do not lead to high conductivity as might be expected for nominally donor defects. In fact, O_N and Si_{Al} in particular have been used to directly control growth polarity of AlN-based films, adding more complexity to the understanding of polarity and domain walls/inversion domain boundaries in these films. Understanding charge and defect distributions at domain walls is a near-term need for both scientific and technological progress of wurtzite ferroelectrics.

Research on wurtzite ferroelectrics is still in its infant stages but the importance of defects is already clear. Emerging evidence has demonstrated the contribution of point defects like nitrogen vacancy and oxygen substitutional defects to leakage current, polarization switching barrier, and breakdown. It remains to be understood if the presence of large concentrations of point defects and small complexes will qualitatively affect the switching mechanisms discussed in Sec. II D.

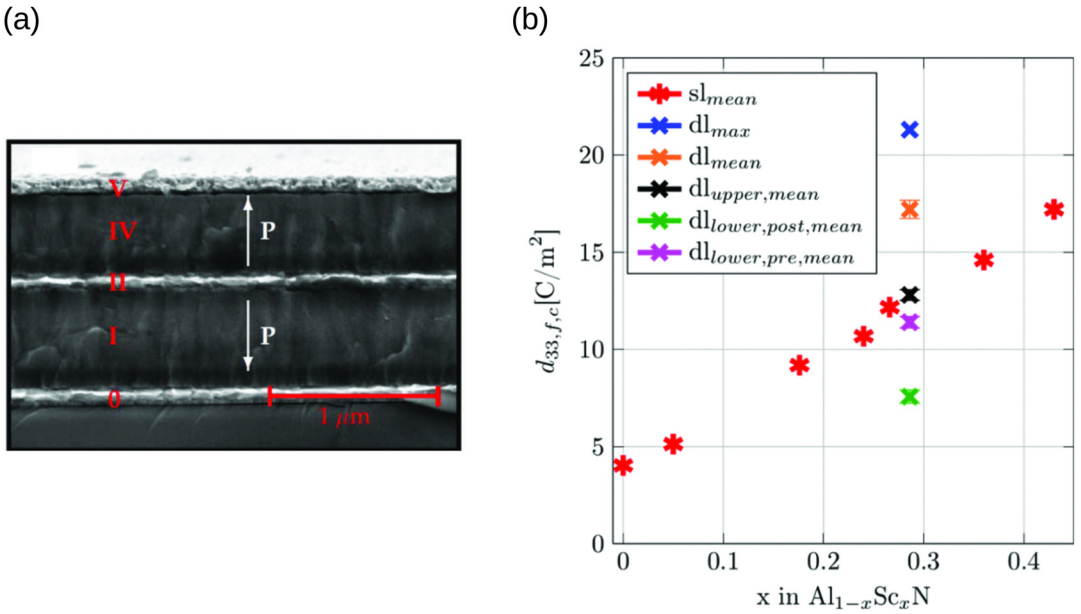

FIG. 20. (a) SEM image of the cross-section of an $Al_{1-x}Sc_xN$-based double layer separated by an intermediate Pt electrode (II) and with opposing polarization directions (I, IV) due to ferroelectric switching. (b) The dependence of the longitudinal piezoelectric coefficient $d_{33,f}$ on the Sc content for a single layer (sl) as well as the effective $d_{33,f}$ for a double layer (dl). The latter was determined for the individual layers only (upper, lower, as-deposited and after FE-switching) as well as in the double layer configuration, exhibiting the highest $d_{33,f}$. Reproduced with permission from Fichtner *et al.*, "A generic CMOS compatible piezoelectric multilayer actuator approach based on permanent ferroelectric polarization inversion in $Al_{1-x}Sc_xN$," in *20th International Conference on Solid-State Sensors, Actuators and Microsystems & Eurosensors XXXIII (TRANSDUCERS & EUROSENSORS XXXIII)* (IEEE, 2019).[144] Copyright 2019 IEEE.

Furthermore, it also remains unclear if the same point defects and complexes will affect domain nucleation and growth. While there are initial hints at the effect of point defects, the role(s) of extended defects, such as stacking faults, grain boundaries and interfaces on domain structures is completely uncharted. Further investigations to mechanistically understand and quantify the effects of defects on dielectric and ferroelectric properties will require collaborative computational and experimental studies and the acquired knowledge can open the door to defect engineering of wurtzite ferroelectrics.

VI. SUMMARY

It took until 2019 for the world to recognize the ability of wurtzite structures to support ferroelectricity, but the community has made rapid progress in the subsequent years in both fundamental understanding and device-relevant integration. For example, we now know the true magnitude of spontaneous polarization in the wurtzite structure and have made significant strides in understanding both the nature and energetics of intermediate states during polarization reversal. Atomic-resolution microscopy shows remarkable agreement with simulated structures of intermediate polarity, and ongoing experimental confirmation of predictions of stability and switching behavior increase confidence for accelerated computationally guided development. Device ideas abound, and proof-of-concept demonstrations of new ideas for leveraging ferroelectric wurzites are pouring out of both academic and industrial research labs.

Continuation of such rapid progress, though, will require a more coherent and comprehensive understanding (and affiliated communication) of defects and compensation during growth, polarization switching, and operation/degradation. The community needs to reconcile the apparent inconsistencies in assumptions and boundary conditions across not just individual studies but communities working in this space. Finally, interfaces—including domain walls of all types, electrode/ferroelectric interfaces, and free surfaces during growth and operation—deserve significantly more attention. With investment in these areas (and certainly more around the corner), the future of wurtzite ferroelectrics is bright.

ACKNOWLEDGMENTS

This collaborative work was supported in part by the Federal Ministry of Education and Research (BMBF) under Project No. 03VP10842 (VIP+ FeelScreen) and the European Union (FIXIT, GA 101135398). Views and opinions expressed are however those of the author(s) only and do not necessarily reflect those of the European Union or the European Research Council Executive Agency. This work was authored in part by the National Renewable Energy Laboratory, operated by Alliance for Sustainable Energy, LLC, for DOE under Contract No. DE-AC36-08GO28308. The views expressed in the article do not necessarily represent the views of the DOE or the U.S. Government. This work was supported by the Deutsche Forschungsgemeinschaft (DFG) under the scheme of the Collaborative Research Center (CRC) 1261-Project ID 458372836. The work was partially supported by the National Science Foundation under Grant No. DMR-2119281. Funding was provided by the Department of Energy Basic Energy Sciences (BES) under Program No. ERW6548.

AUTHOR DECLARATIONS

Conflict of Interest

The authors have no conflicts to disclose.

Author Contributions

Simon Fichtner: Conceptualization (equal); Funding acquisition (equal); Project administration (equal); Resources (equal); Supervision (equal); Writing – original draft (equal); Writing – review & editing (equal). **Georg Schönweger:** Writing – original draft (equal); Writing – review & editing (equal). **Cheng-Wei Lee:** Writing – original draft (equal); Writing – review & editing (equal). **Keisuke Yazawa:** Conceptualization (supporting); Funding acquisition (supporting); Writing – original draft (equal); Writing – review & editing (equal). **Prashun Gorai:** Conceptualization (equal); Funding acquisition (equal); Resources (equal); Supervision (equal); Writing – original draft (equal); Writing – review & editing (equal). **Geoff L. Brennecka:** Conceptualization (equal); Funding acquisition (equal); Project administration (equal); Resources (equal); Supervision (equal); Writing – original draft (equal); Writing – review & editing (equal).

DATA AVAILABILITY

Data sharing is not applicable to this article as no new data were created or analyzed in this study.

REFERENCES

[1]S. Fichtner, N. Wolff, F. Lofink, L. Kienle, and B. Wagner, J. Appl. Phys. **125**, 114103 (2019).
[2]T. S. Böscke, J. Müller, D. Bräuhaus, U. Schröder, and U. Böttger, Appl. Phys. Lett. **99**, 102903 (2011).
[3]D. Jena, R. Page, J. Casamento, P. Dang, J. Singhal, Z. Zhang, J. Wright, G. Khalsa, Y. Cho, and H. G. Xing, Jpn. J. Appl. Phys. **58**, SC0801 (2019).
[4]D. Wang, S. Yang, J. Liu, D. Wang, and Z. Mi, Appl. Phys. Lett. **124**, 150501 (2024).
[5]K. H. Kim, I. Karpov, R. H. Olsson, and D. Jariwala, Nat. Nanotechnol. **18**, 422–441 (2023).
[6]F. Yang, Adv. Electron. Mater. **11**, 2400279 (2024).
[7]R. Ramesh and D. G. Schlom, Nat. Rev. Mater. **4**, 257–268 (2019).
[8]L. Qi, S. Ruan, and Y. J. Zeng, Adv. Mater. **33**, 2005098 (2021).
[9]F. Li, M. J. Cabral, B. Xu, Z. Cheng, E. C. Dickey, J. M. LeBeau, J. Wang, J. Luo, S. Taylor, W. Hackenberger, L. Bellaiche, Z. Xu, L. Q. Chen, T. R. Shrout, and S. Zhang, Science **364**, 264–268 (2019).
[10]R. Resta, Rev. Mod. Phys. **66**(3), 899–915 (1994).
[11]R. D. King-Smith and D. Vanderbilt, Phys. Rev. B **47**(3), 1651–1654 (1993).
[12]N. A. Spaldin, J. Solid State Chem. **195**, 2–10 (2012).
[13]C. E. Dreyer, A. Janotti, C. G. Van de Walle, and D. Vanderbilt, Phys. Rev. X **6**, 021038 (2016).
[14]W. J. Merz, Phys. Rev. **95**(3), 690–698 (1954).
[15]G. Catalan, J. Seidel, R. Ramesh, and J. F. Scott, Rev. Mod. Phys. **84**(1), 119–156 (2012).
[16]G. Sanchez-Santolino, J. Tornos, D. Hernandez-Martin, J. I. Beltran, C. Munuera, M. Cabero, A. Perez-Muñoz, J. Ricote, F. Mompean, M. Garcia-Hernandez, Z. Sefrioui, C. Leon, S. J. Pennycook, M. C. Muñoz, M. Varela, and J. Santamaria, Nat. Nanotechnol. **12**, 655–662 (2017).
[17]C. T. Nelson, R. K. Vasudevan, X. Zhang, M. Ziatdinov, E. A. Eliseev, I. Takeuchi, A. N. Morozovska, and S. V. Kalinin, Nat. Commun. **11**, 6361 (2020).
[18]Y. Ivry, J. F. Scott, E. K. H. Salje, and C. Durkan, Phys. Rev. B **86**(20), 205428 (2012).
[19]D. Meier and S. M. Selbach, Nat. Rev. Mater. **7**, 157–173 (2021).
[20]J. Seidel, L. W. Martin, Q. He, Q. Zhan, Y. H. Chu, A. Rother, M. E. Hawkridge, P. Maksymovych, P. Yu, M. Gajek, N. Balke, S. V. Kalinin, S. Gemming, F. Wang, G. Catalan, J. F. Scott, N. A. Spaldin, J. Orenstein, and R. Ramesh, Nat. Mater. **8**, 229–234 (2009).
[21]M. R. Islam, N. Wolff, M. Yassine, G. Schönweger, B. Christian, H. Kohlstedt, O. Ambacher, F. Lofink, L. Kienle, and S. Fichtner, Appl. Phys. Lett. **118**, 232905 (2021).
[22]H. Moriwake, A. Konishi, T. Ogawa, K. Fujimura, C. A. J. Fisher, A. Kuwabara, T. Shimizu, S. Yasui, and M. Itoh, Appl. Phys. Lett. **104**, 242909 (2014).
[23]H. Blank, P. Delavignette, R. Gevers, and S. Amelinckx, Phys. Status Solidi (b) **7**, 747–764 (1964).
[24]L. T. Romano, J. E. Northrup, and M. A. O'Keefe, Appl. Phys. Lett. **69**, 2394–2396 (1996).
[25]S. Mohn, N. Stolyarchuk, T. Markurt, R. Kirste, M. P. Hoffmann, R. Collazo, A. Courville, R. Di Felice, Z. Sitar, P. Vennéguès, and M. Albrecht, Phys. Rev. Appl. **5**, 054004 (2016).
[26]J. F. Scott, Ferroelectrics **503**, 117–132 (2016).
[27]L. Li, L. Xie, and X. Pan, Rep. Prog. Phys. **82**, 126502 (2019).
[28]M. G. Han, M. S. Marshall, L. Wu, M. A. Schofield, T. Aoki, R. Twesten, J. Hoffman, F. J. Walker, C. H. Ahn, and Y. Zhu, Nat. Commun. **5**, 4693 (2014).
[29]T. Denneulin and A. S. Everhardt, J. Phys.: Condens. Matter **34**, 235701 (2022).
[30]S. Calderon, J. Hayden, S. M. Baksa, W. Tzou, S. Trolier-McKinstry, I. Dabo, J. P. Maria, and E. C. Dickey, Science **380**, 1034–1038 (2023).
[31]G. Schönweger, N. Wolff, M. R. Islam, M. Gremmel, A. Petraru, L. Kienle, H. Kohlstedt, and S. Fichtner, Adv. Sci. **10**, 2302296 (2023).
[32]D. Wang, D. Wang, M. Molla, Y. Liu, S. Yang, M. Hu, J. Liu, Y. Wu, T. Ma, E. Kioupakis, and Z. Mi, "Electric-field-induced domain walls in wurtzite ferroelectrics," arXiv:2312.08645.
[33]J. Hayden, M. D. Hossain, Y. Xiong, K. Ferri, W. Zhu, M. V. Imperatore, N. Giebink, S. Trolier-McKinstry, I. Dabo, and J. P. Maria, Phys. Rev. Mater. **5**, 044412 (2021).
[34]D. Wang, S. Mondal, J. Liu, M. Hu, P. Wang, S. Yang, D. Wang, Y. Xiao, Y. Wu, T. Ma, and Z. Mi, Appl. Phys. Lett. **123**, 033504 (2023).
[35]K. Ferri, S. Bachu, W. Zhu, M. Imperatore, J. Hayden, N. Alem, N. Giebink, S. Trolier-McKinstry, and J. P. Maria, J. Appl. Phys **130**, 044101 (2021).
[36]M. Uehara, R. Mizutani, S. Yasuoka, T. Shiraishi, T. Shimizu, H. Yamada, M. Akiyama, and H. Funakubo, Appl. Phys. Lett. **119**, 172901 (2021).
[37]D. Wang, P. Wang, B. Wang, and Z. Mi, Appl. Phys. Lett. **119**, 111902 (2021).
[38]C. W. Lee, R. W. Smaha, G. L. Brennecka, N. Haegel, P. Gorai, and K. Yazawa, "From prediction to experimental realization of ferroelectric wurtzite $Al_{1-x}Gd_xN$ alloys," arXiv:2407.11262v1 (2024).
[39]C. W. Lee, K. Yazawa, A. Zakutayev, G. L. Brennecka, and P. Gorai, Sci. Adv. **10**, eadl0848 (2024).
[40]C. W. Lee, N. U. Din, K. Yazawa, G. L. Brennecka, A. Zakutayev, and P. Gorai, Matter **7**, 1644–1659 (2024).
[41]Z. Liu, X. Wang, X. Ma, Y. Yang, and D. Wu, Appl. Phys. Lett. **122**, 122901 (2023).
[42]G. Henkelman, B. P. Uberuaga, and H. Jónsson, J. Chem. Phys. **113**, 9901–9904 (2000).
[43]D. Sheppard, P. Xiao, W. Chemelewski, D. D. Johnson, and G. Henkelman, J. Chem. Phys **136**, 074103 (2012).
[44]Y. Dai and M. Wu, Sci. Adv. **9**, eadf8706 (2023).
[45]K. H. Ye, G. Han, I. W. Yeu, C. S. Hwang, and J. H. Choi, Phys. Status Solidi **15**, 2100009 (2021).
[46]A. J. E. Rowberg, S. Mu, M. W. Swift, and C. G. Van de Walle, Phys. Rev. Mater. **5**(9), 094602 (2021).
[47]S. M. Baksa, S. Gelin, S. Oturak, R. J. Spurling, A. Sepehrinezhad, L. Jacques, S. E. Trolier-McKinstry, A. C. T. van Duin, J. P. Maria, A. M. Rappe, and I. Dabo, Adv. Electron. Mater. (published online 2024).
[48]D. Behrendt, V. B. Nascimento, and A. M. Rappe, Phys. Rev. B **110**(3), 035204 (2024).
[49]D. Behrendt, A. Samanta, and A. M. Rappe, "Ferroelectric fractals: Switching mechanism of wurtzite AlN," arXiv:2410.18816 (2024).
[50]K. Yazawa, J. S. Mangum, P. Gorai, G. L. Brennecka, and A. Zakutayev, J. Mater. Chem. C **10**, 17557–17566 (2022).
[51]J. Jia, D. Kishi, N. Bai, T. Okajima, F. Lesari, and T. Yanagitani, Phys. Rev. B **109**, 134101 (2024).
[52]H. Moriwake, R. Yokoi, A. Taguchi, T. Ogawa, C. A. J. Fisher, A. Kuwabara, Y. Sato, T. Shimizu, Y. Hamasaki, H. Takashima, and M. Itoh, APL Mater. **8**(532X), 121102 (2020).

[53]M. Hu, X. Yang, T. Su, X. Ma, and W. Ren, Appl. Phys. Lett. **118**, 122903 (2021).
[54]X. Y. Chen, J. L. Yang, L. F. Chen, H. K. Xu, J. M. Chen, G. X. Lai, X. F. Xu, H. Ji, J. J. Tang, and Y. J. Zhao, Phys. Chem. Chem. Phys. **24**(48), 29570–29578 (2022).
[55]R. A. Young and W. T. Ziegler, J. Am. Chem. Soc. **74**, 5251–5253 (1952).
[56]B. Krause, D. S. Kuznetsov, A. E. Yakshin, S. Ibrahimkutty, T. Baumbach, and F. Bijkerk, J. Appl. Crystallogr. **51**, 1013–1020 (2018).
[57]C. Kim, G. Pilania, and R. Ramprasad, Chem. Mater. **28**, 1304–1311 (2016).
[58]J. Breternitz and S. Schorr, Acta Crystallogr., Sect. A **77**, 208–216 (2021).
[59]S. Yasuhara, A. Nakagawa, K. Okamoto, T. Shiraishi, H. Funakubo, S. Yasui, M. Itoh, T. Tsurumi, and T. Hoshina, RSC Adv. **14**(20), 13900–13904 (2024).
[60]K. Yazawa, J. Hayden, J. P. Maria, W. Zhu, S. Trolier-McKinstry, A. Zakutayev, and G. L. Brennecka, Mater. Horiz. **10**, 2936–2944 (2023).
[61]A. N. Kolmogorov, Izv. Akad. Nauk SSSR, Ser. Mat. **3**, 355–359 (1937).
[62]W. Johnson and R. F. Mehl, "Reaction kinetics in processes of nucleation and growth," Technical Report, 1939.
[63]M. Avrami, J. Chem. Phys. **7**, 1103–1112 (1939).
[64]M. Avrami, J. Chem. Phys. **8**, 212–224 (1940).
[65]M. Avrami, J. Chem. Phys. **9**, 177–184 (1941).
[66]Y. Ishibashi and Y. Takagi, J. Phys. Soc. Jpn. **31**, 506–510 (1971).
[67]V. Shur, E. Rumyantsev, and S. Makarov, J. Appl. Phys. **84**, 445–451 (1998).
[68]A. K. Tagantsev, I. Stolichnov, N. Setter, J. S. Cross, and M. Tsukada, Phys. Rev. B **66**, 214109 (2002).
[69]J. Y. Jo, H. S. Han, J. G. Yoon, T. K. Song, S. H. Kim, and T. W. Noh, Phys. Rev. Lett. **99**, 267602 (2007).
[70]T. Y. Lee, K. Lee, H. H. Lim, M. S. Song, S. M. Yang, H. K. Yoo, D. I. Suh, Z. Zhu, A. Yoon, M. R. Macdonald, X. Lei, H. Y. Jeong, D. Lee, K. Park, J. Park, and S. C. Chae, ACS Appl. Mater. Interfaces **11**, 3142–3149 (2019).
[71]S. Fichtner, F. Lofink, B. Wagner, G. Schonweger, T. N. Kreutzer, A. Petraru, and H. Kohlstedt, "Ferroelectricity in AlScN: Switching, imprint and sub-150 nm films," in *Proceedings of the IFCS-ISAF 2020—Joint Conference of the IEEE International Frequency Control Symposium and IEEE International Symposium on Applications of Ferroelectrics* (Institute of Electrical and Electronics Engineers Inc., 2020).
[72]R. Guido, H. Lu, P. D. Lomenzo, T. Mikolajick, A. Gruverman, and U. Schroeder, Adv. Sci. **11**, 2308797 (2024).
[73]J. Wu, J. Wang, D. Xiao, and J. Zhu, J. Alloys Compd. **509**, L319–L323 (2011).
[74]F. C. Kartawidjaja, C. H. Sim, and J. Wang, J. Appl. Phys. **102**, 124102 (2007).
[75]M. Dawber and J. F. Scott, Appl. Phys. Lett. **76**, 1060–1062 (2000).
[76]J. F. Scott and M. Dawber, Appl. Phys. Lett. **76**, 3801–3803 (2000).
[77]S. Mueller, J. Muller, U. Schroeder, and T. Mikolajick, IEEE Trans. Device Mater. Reliab. **13**, 93–97 (2013).
[78]D. Zhou, J. Xu, Q. Li, Y. Guan, F. Cao, X. Dong, J. Müller, T. Schenk, and U. Schröder, Appl. Phys. Lett. **103**, 192904 (2013).
[79]F. P. G. Fengler, M. Pešić, S. Starschich, T. Schneller, C. Künneth, U. Böttger, H. Mulaosmanovic, T. Schenk, M. H. Park, R. Nigon, P. Muralt, T. Mikolajick, and U. Schroeder, Adv. Electron. Mater. **3**, 1600505 (2017).
[80]W. Zhu, F. He, J. Hayden, Z. Fan, J. I. Yang, J. Maria, and S. Trolier-McKinstry, Adv. Electron. Mater. **8**, 2100931 (2022).
[81]K. Yazawa, D. Drury, J. Hayden, J. Maria, S. Trolier-McKinstry, A. Zakutayev, and G. L. Brennecka, J. Am. Ceram. Soc. **107**, 1523–1532 (2023).
[82]D. Wang, J. Zheng, Z. Tang, M. D'Agati, P. S. Gharavi, X. Liu, D. Jariwala, E. A. Stach, R. H. Olsson, V. Roebisch, M. Kratzer, B. Heinz, M. G. Han, and K. Kisslinger, "Ferroelectric C-axis textured aluminum scandium nitride thin films of 100 nm thickness," in *Proceedings of the IFCS-ISAF 2020—Joint Conference of the IEEE International Frequency Control Symposium and IEEE International Symposium on Applications of Ferroelectrics* (Institute of Electrical and Electronics Engineers Inc., 2020).
[83]F. He, W. Zhu, J. Hayden, J. Casamento, Q. Tran, K. Kang, Y. Song, B. Akkopru-Akgun, J. I. Yang, P. Tipsawat, G. Brennecka, S. Choi, T. N. Jackson, J. P. Maria, and S. Trolier-McKinstry, Acta Mater. **266**, 119678 (2024).
[84]S. M. Chen, T. Hoshii, H. Wakabayashi, K. Tsutsui, E. Y. Chang, and K. Kakushima, Jpn. J. Appl. Phys. **63**, 03SP45 (2024).
[85]K. D. Kim, Y. B. Lee, S. H. Lee, I. S. Lee, S. K. Ryoo, S. Y. Byun, J. H. Lee, and C. S. Hwang, Nanoscale **15**(40), 16390–16402 (2023).
[86]G. Schönweger, A. Petraru, M. R. Islam, N. Wolff, B. Haas, A. Hammud, C. Koch, L. Kienle, H. Kohlstedt, and S. Fichtner, Adv. Funct. Mater. **32**(3028), 2109632 (2022).
[87]M. Gremmel and S. Fichtner, J. Appl. Phys. **135**, 204101 (2024).
[88]W. Zhu, J. Hayden, F. He, J. I. Yang, P. Tipsawat, M. D. Hossain, J. P. Maria, and S. Trolier-McKinstry, Appl. Phys. Lett. **119**, 062901 (2021).
[89]D. Drury, K. Yazawa, A. Zakutayev, B. Hanrahan, and G. Brennecka, Micromachines **13**, 887 (2022).
[90]U. Mishra, S. Likun, T. Kazior, and Y. F. Wu, Proc. IEEE **96**, 287–305 (2008).
[91]R. Gaska, G. Simin, and M. Shur, "AlGaN/GaN HEMTs for energy efficient systems," in *2013 IEEE Energytech* (IEEE, 2013), pp. 1–6.
[92]N. Islam, M. F. P. Mohamed, M. F. A. J. Khan, S. Falina, H. Kawarada, and M. Syamsul, Crystals **12**, 1581 (2022).
[93]U. Mishra, P. Parikh, and Y. F. Wu, Proc. IEEE **90**, 1022–1031 (2002).
[94]M. Akiyama, T. Kamohara, K. Kano, A. Teshigahara, Y. Takeuchi, and N. Kawahara, Adv. Mater. **21**, 593–596 (2009).
[95]G. Wingqvist, F. Tasnádi, A. Zukauskaite, J. Birch, H. Arwin, and L. Hultman, Appl. Phys. Lett. **97**, 112902 (2010).
[96]W. Wang, P. M. Mayrhofer, X. He, M. Gillinger, Z. Ye, X. Wang, A. Bittner, U. Schmid, and J. K. Luo, Appl. Phys. Lett. **105**, 133502 (2014).
[97]A. Žukauskaitė, Micromachines **14**, 1067 (2023).
[98]J. Y. Yang, S. Y. Oh, M. J. Yeom, S. Kim, G. Lee, K. Lee, S. Kim, and G. Yoo, IEEE Electron Device Lett. **44**, 1260–1263 (2023).
[99]J. Casamento, K. Nomoto, T. S. Nguyen, H. Lee, C. Savant, L. Li, A. Hickman, T. Maeda, J. Encomendero, V. Gund, A. Lal, J. C. M. Hwang, H. G. Xing, and D. Jena, "FerroHEMTs: High-current and high-speed all-epitaxial AlScN/GaN ferroelectric transistors," in *International Electron Devices Meeting (IEDM)* (IEEE, 2022).
[100]D. Wang, P. Wang, M. He, J. Liu, S. Mondal, M. Hu, D. Wang, Y. Wu, T. Ma, and Z. Mi, Appl. Phys. Lett. **122**, 090601 (2023).
[101]V. Gund, K. Nomoto, H. G. Xing, D. Jena, and A. Lal, "Intrinsically switchable GHz ferroelectric ScALN SAW resonators," in *IEEE International Symposium on Applications of Ferroelectrics (ISAF)* (IEEE, 2022).
[102]J. Wang, M. Park, S. Mertin, T. Pensala, F. Ayazi, and A. Ansari, J. Microelectromech. Syst. **29**, 741–747 (2020).
[103]K. H. Kim, S. Oh, M. M. A. Fiagbenu, J. Zheng, P. Musavigharavi, P. Kumar, N. Trainor, A. Aljarb, Y. Wan, H. M. K. K. Kim, S. Song, G. Kim, Z. Tang, J. H. Fu, M. Hakami, V. Tung, J. M. Redwing, E. A. Stach, R. H. Olsson, and D. Jariwala, Nat. Nanotechnol. **18**, 1044–1050 (2023).
[104]N. Sun, K. Okamoto, S. Yasuoka, S. Doko, N. Matsui, T. Irisawa, K. Tsunekawa, T. Katase, T. Koganezawa, T. Nakatani, R. Kumara, O. Sakata, and H. Funakubo, Appl. Phys. Lett. **125**, 032904 (2024).
[105]G. Schönweger, M. R. Islam, and S. Fichtner, "Structural and ferroelectric properties of $Al_{1-x}Sc_xN$," in *Semiconductors and Semimetals* (Elsevier, 2023), Vol. 114, pp. 71–99.
[106]P. Wang, D. Wang, N. M. Vu, T. Chiang, J. T. Heron, and Z. Mi, Appl. Phys. Lett. **118**, 223504 (2021).
[107]P. Wang, D. Wang, S. Mondal, and Z. Mi, Appl. Phys. Lett. **121**, 023501 (2022).
[108]D. Wang, P. Wang, S. Mondal, Y. Xiao, M. Hu, and Z. Mi, Appl. Phys. Lett. **121**, 042108 (2022).
[109]N. Wolff, G. Schönweger, I. Streicher, M. R. Islam, N. Braun, P. Straňák, L. Kirste, M. Prescher, A. Lotnyk, H. Kohlstedt, S. Leone, L. Kienle, and S. Fichtner, Adv. Phys. Res. **3**, 2300113 (2024).
[110]G. Schönweger, M. R. Islam, N. Wolff, A. Petraru, L. Kienle, H. Kohlstedt, and S. Fichtner, Phys. Status Solidi **17**, 2200312 (2023).
[111]S. Yasuoka, T. Shimizu, A. Tateyama, M. Uehara, H. Yamada, M. Akiyama, Y. Hiranaga, Y. Cho, and H. Funakubo, J. Appl. Phys. **128**, 114103 (2020).
[112]J. X. Zheng, M. M. A. Fiagbenu, G. Esteves, P. Musavigharavi, A. Gunda, D. Jariwala, E. A. Stach, and R. H. Olsson, Appl. Phys. Lett. **122**, 222901 (2023).
[113]N. Wolff, S. Fichtner, B. Haas, M. R. Islam, F. Niekiel, M. Kessel, O. Ambacher, C. Koch, B. Wagner, F. Lofink, and L. Kienle, J. Appl. Phys. **129**, 034103 (2021).
[114]S. Yu, Proc. IEEE **106**, 260–285 (2018).
[115]E. Covi, H. Mulaosmanovic, B. Max, S. Slesazeck, and T. Mikolajick, Neuromorph. Comput. Eng. **2**, 012002 (2022).

[116]S. Fichtner, G. Schönweger, F. Dietz, H. Hanssen, H. Züge, T. N. Kreutzer, F. Lofink, H. Kohlstedt, H. Kapels, and M. Mensing, "Wurtzite-type ferroelectrics for microelectronic devices: Scalability and integration to silicon based ferroelectric FETs," in *7th IEEE Electron Devices Technology & Manufacturing Conference (EDTM)* (IEEE, 2023), pp. 1–3.
[117]D. Wang, P. Wang, S. Mondal, M. Hu, Y. Wu, T. Ma, and Z. Mi, Adv. Mater. **35**, 2210628 (2023).
[118]Y. He, S. Chen, M. M. A. Fiagbenu, C. Leblanc, P. Musavigharavi, G. Kim, X. Du, J. Chen, X. Liu, E. A. Stach, R. H. Olsson, and D. Jariwala, Appl. Phys. Lett. **123**, 122901 (2023).
[119]D. Wang, P. Wang, S. Mondal, S. Mohanty, T. Ma, E. Ahmadi, and Z. Mi, Adv. Electron. Mater. **8**, 2200005 (2022).
[120]X. Liu, J. Zheng, D. Wang, P. Musavigharavi, E. A. Stach, R. Olsson, and D. Jariwala, Appl. Phys. Lett. **118**, 202901 (2021).
[121]M. Liu, S. Lu, Y. Jia, H. Zang, K. Jiang, X. Sun, and D. Li, IEEE Electron Device Lett. **45**(3), 356–359 (2023).
[122]H. Mulaosmanovic, J. Ocker, S. Müller, U. Schroeder, J. Müller, P. Polakowski, S. Flachowsky, R. van Bentum, T. Mikolajick, and S. Slesazeck, ACS Appl. Mater. Interfaces **9**, 3792–3798 (2017).
[123]M. T. Hardy, B. P. Downey, N. Nepal, D. F. Storm, D. S. Katzer, and D. J. Meyer, Appl. Phys. Lett. **110**, 162104 (2017).
[124]O. Ambacher, A. Yassine, M. Yassine, S. Mihalic, E. Wade, and B. Christian, J. Appl. Phys. **131**, 245702 (2022).
[125]J. Casamento, T. S. Nguyen, Y. Cho, C. Savant, T. Vasen, S. Afroz, D. Hannan, H. G. Xing, and D. Jena, Appl. Phys. Lett. **121**, 192101 (2022).
[126]D. M. Evans, V. Garcia, D. Meier, and M. Bibes, Phys. Sci. Rev. **5**, 20190067 (2020).
[127]H. Lu, G. Schönweger, A. Petraru, H. Kohlstedt, S. Fichtner, and A. Gruverman, Adv. Funct. Mater. **34**, 2315169 (2024).
[128]J. P. V. McConville, H. Lu, B. Wang, Y. Tan, C. Cochard, M. Conroy, K. Moore, A. Harvey, U. Bangert, L. Q. Chen, A. Gruverman, and J. M. Gregg, Adv. Funct. Mater. **30**, 2000109 (2020).
[129]P. Sharma, Q. Zhang, D. Sando, C. H. Lei, Y. Liu, J. Li, V. Nagarajan, and J. Seidel, Sci. Adv. **3**, e1700512 (2017).
[130]T. Sluka, A. K. Tagantsev, P. Bednyakov, and N. Setter, Nat. Commun. **4**, 1808 (2013).
[131]C. S. Werner, S. J. Herr, K. Buse, B. Sturman, E. Soergel, C. Razzaghi, and I. Breunig, Sci. Rep. **7**, 9862 (2017).
[132]J. Sun, Y. Li, D. Hu, B. Shen, B. Zhang, Z. Wang, H. Tang, and A. Jiang, Microstructures **4**, 2024007 (2024).
[133]D. S. Hum and M. M. Fejer, C. R. Phys. **8**, 180–198 (2006).
[134]Z. Tang, G. Esteves, and R. H. Olsson, J. Appl. Phys. **134**, 144101 (2023).
[135]V. Yoshioka, J. Lu, Z. Tang, J. Jin, R. H. Olsson, and B. Zhen, APL Mater. **9**, 101104 (2021).
[136]F. Yang, G. Yang, D. Wang, P. Wang, J. Lu, Z. Mi, and H. X. Tang, Appl. Phys. Lett. **123**, 101103 (2023).
[137]E. Courjon, N. Courjal, W. Daniau, G. Lengaigne, L. Gauthier-Manuel, S. Ballandras, and J. Hauden, J. Appl. Phys. **102**, 114107 (2007).
[138]Y. F. Chen, S. N. Zhu, Y. Y. Zhu, N. B. Ming, B. B. Jin, and R. X. Wu, Appl. Phys. Lett. **70**, 592–594 (1997).
[139]S. Rassay, D. Mo, and R. Tabrizian, Micromachines **13**, 1003 (2022).
[140]M. Fejer, G. Magel, D. Jundt, and R. Byer, IEEE J. Quantum Electron. **28**, 2631–2654 (1992).
[141]S. Takahashi, Jpn. J. Appl. Phys. **24**, 41 (1985).
[142]C. A. Randall, A. Kelnberger, G. Y. Yang, R. E. Eitel, and T. R. Shrout, J. Electroceram. **14**, 177–191 (2005).
[143]N. Ishii and T. Yanagitani, "Polarization inverted two layer ScAlN thin film resonator fabricated by applying external electric field," in *IEEE International Ultrasonics Symposium (IUS)* (IEEE, Venice, Italy, 2022), pp. 1–4.
[144]S. Fichtner, D. Kaden, F. Lofink, and B. Wagner, "A generic CMOS compatible piezoelectric multilayer actuator approach based on permanent ferroelectric polarization inversion in $Al_{1-x}Sc_xN$," in *20th International Conference on Solid-State Sensors, Actuators and Microsystems & Eurosensors XXXIII (TRANSDUCERS & EUROSENSORS XXXIII)* (IEEE, 2019).
[145]T. N. Kreutzer, S. Fichtner, B. Wagner, and F. Lofink, "A double-layer MEMS actuator based on ferroelectric polarization inversion in AlScN," in *IEEE International Symposium on Applications of Ferroelectrics (ISAF)* (IEEE, 2021), pp. 1–3.
[146]Y. Feng, J. Wu, Q. Chi, W. Li, Y. Yu, and W. Fei, Chem. Rev. **120**, 1710–1787 (2020).
[147]M. H. Park, D. H. Lee, K. Yang, J. Y. Park, G. T. Yu, H. W. Park, M. Materano, T. Mittmann, P. D. Lomenzo, T. Mikolajick, U. Schroeder, and C. S. Hwang, J. Mater. Chem. C **8**(31), 10526–10550 (2020).
[148]Y. A. Genenko, J. Glaum, M. J. Hoffmann, and K. Albe, Mater. Sci. Eng., B **192**, 52–82 (2015).
[149]S. Jesse, B. J. Rodriguez, S. Choudhury, A. P. Baddorf, I. Vrejoiu, D. Hesse, M. Alexe, E. A. Eliseev, A. N. Morozovska, J. Zhang, L. Q. Chen, and S. V. Kalinin, Nat. Mater. **7**, 209–215 (2008).
[150]C. W. Lee, N. U. Din, K. Yazawa, W. Nemeth, R. W. Smaha, N. M. Haegel, and P. Gorai, J. Appl. Phys. **135**, 155101 (2024).
[151]C. W. Lee, N. U. Din, G. L. Brennecka, and P. Gorai, Appl. Phys. Lett. **125**, 022901 (2024).
[152]S. L. Tsai, T. Hoshii, H. Wakabayashi, K. Tsutsui, T. K. Chung, E. Y. Chang, and K. Kakushima, Jpn. J. Appl. Phys. **61**, SJ1005 (2022).
[153]R. Guido, T. Mikolajick, U. Schroeder, and P. D. Lomenzo, Nano Lett. **23**, 7213–7220 (2023).
[154]T. Mayeshiba and D. Morgan, Phys. Chem. Chem. Phys. **17**(4), 2715–2721 (2015).
[155]Q. Ren, X. Liu, Z. Ding, Y. Liu, Q. Zhou, Q. Qian, G. Zhang, H. Li, and N. Wang, ACS Appl. Mater. Interfaces **16**, 28838–28844 (2024).
[156]M. Akiyama, T. Kamohara, K. Kano, A. Teshigahara, and N. Kawahara, Appl. Phys. Lett. **93**, 021903 (2008).
[157]S. A. Anggraini, M. Uehara, K. Hirata, H. Yamada, and M. Akiyama, Sci. Rep. **10**, 4369 (2020).
[158]M. Uehara, H. Shigemoto, Y. Fujio, T. Nagase, Y. Aida, K. Umeda, and M. Akiyama, Appl. Phys. Lett. **111**, 112901 (2017).